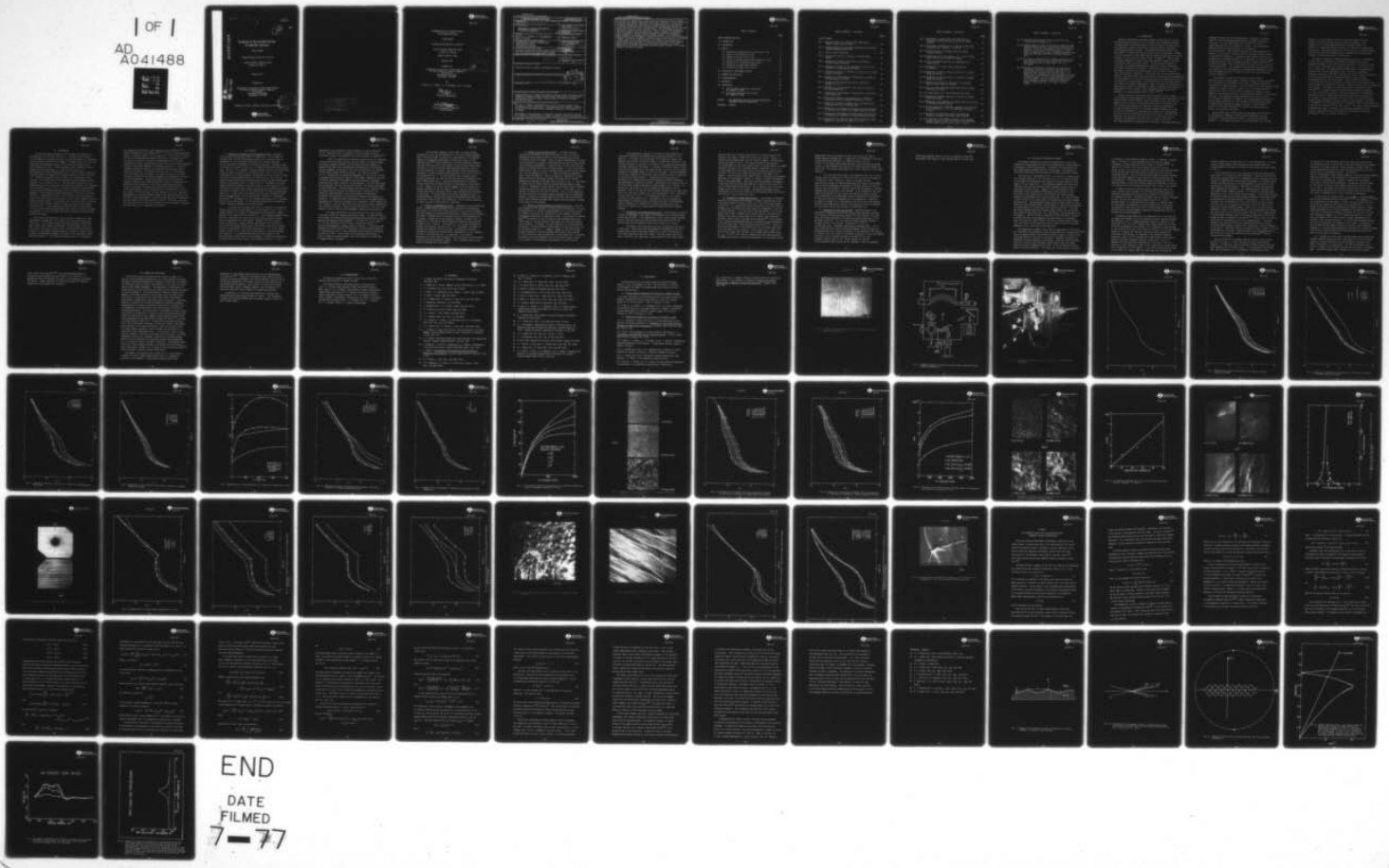
AD-A041 488 ROCKWELL INTERNATIONAL THOUSAND OAKS CALIF SCIENCE --ETC F/G 13/13
MECHANISMS OF EXO-ELECTRON EMISSION IN STRUCTURAL MATERIALS.(U)
FEB 77 O BUCK, W J PARDEE, F J SZALKOWSKI F44620-74-C-0043
UNCLASSIFIED SC573.5FR AFOSR-TR-77-0766 NL

| OF |
AD
A041488



END

DATE
FILMED
7-77

AFOSR-TR- 77-0766

SC573.5FR

19

AD A041488

MECHANISMS OF EXO-ELECTRON EMISSION IN STRUCTURAL MATERIALS

FINAL REPORT

Covering Period 01/01/74 to 12/31/76

Contract Number F44620-74-C-0043
Project No. 9761-02

February 1977

AD No.
DDC FILE COPY

Prepared for

Directorate of Electronic & Solid State Sciences
Air Force Office of Scientific Research
Building 410
Bolling Air Force Base
Washington, DC 20332

DDC
RECEIVED
JUL 11 1977
C

Approved for public release; distribution unlimited.

Science Center
Rockwell International

AIR FORCE OFFICE OF SCIENTIFIC RESEARCH (AFSC)
NOTICE OF TRANSMITTAL TO DDC
This technical report has been reviewed and is
approved for public release IAW AFR 190-12 (7b).
Distribution is unlimited.
A. D. BLOSE
Technical Information Officer

Science Center
Rockwell International

SC573.5FR

MECHANISMS OF EXO-ELECTRON EMISSION IN STRUCTURAL MATERIALS

FINAL REPORT

Covering Period 01/01/74 to 12/31/76

Contract Number F44620-74-C-0043
Project No. 9761-02
General Order No. 5068

February 1977



Prepared for:

Directorate of Electronic & Solid State Sciences
Air Force Office of Scientific Research
Building 410
Bolling Air Force Base
Washington, DC 20332

By:

O. Buck, W. J. Pardee, F. J. Szalkowski, and J. M. Curnow

O. Buck
Principal Investigator

D. O. Thompson
Director, Structural Materials
Program Manager

UNCLASSIFIED

SECURITY CLASSIFICATION OF THIS PAGE *(When Data Entered)*

(19) REPORT DOCUMENTATION PAGE	READ INSTRUCTIONS BEFORE COMPLETING FORM
1. REPORT NUMBER (18) AFOSR-TR-77-0766	2. GOVT ACCESSION NO. / 3. RECIPIENT'S CATALOG NUMBER
4. TITLE *(and Subtitle)* (6) MECHANISMS OF EXO-ELECTRON EMISSION IN STRUCTURAL MATERIALS,	5. TYPE OF REPORT & PERIOD COVERED Final Report 01/01/74 to 12/31/76
	6. PERFORMING ORG. REPORT NUMBER (14) SC573.5FR
7. AUTHOR(s) (10) O. Buck, W. J. Pardee, F. J. Szalkowski and J. M. Curnow	8. CONTRACT OR GRANT NUMBER(s) (15) F44620-74-C-0043 new
9. PERFORMING ORGANIZATION NAME AND ADDRESS Science Center, Rockwell International 1049 Camino Dos Rios Thousand Oaks, CA 91360	10. PROGRAM ELEMENT, PROJECT, TASK AREA & WORK UNIT NUMBERS Proj. No. 9761-02 (16) 61102F (17) 02
11. CONTROLLING OFFICE NAME AND ADDRESS Director of Electronics & Solid State Sciences Air Force Office of Scientific Research (AFSC) Bldg. 410, Bolling AFB, Washington, DC 20332	12. REPORT DATE (11) February 1977
	13. NUMBER OF PAGES 82
14. MONITORING AGENCY NAME & ADDRESS *(if different from Controlling Office)* (12) 82 p.	15. SECURITY CLASS. *(of this report)* Unclassified
	15a. DECLASSIFICATION/ DOWNGRADING SCHEDULE N/A

16. DISTRIBUTION STATEMENT *(of this Report)*

Approved for public release; distribution unlimited.

DDC RECEIVED JUL 11 1977 C

17. DISTRIBUTION STATEMENT *(of the abstract entered in Block 20, if different from Report)*

(9) Final rept. 1 Jan 74 - 31 Dec 76

18. SUPPLEMENTARY NOTES

19. KEY WORDS *(Continue on reverse side if necessary and identify by block number)*

Fatigue (Materials), Fatigue Life, Metals, Aluminum, Nickel, Titanium, Surface Properties, Roughness, Oxides, Clean Surfaces, Photo Emissivity, Electrons, Exo-Electrons, Electron Energy, Plasmons, Optical Properties, Scanning Electron Microscope.

20. ABSTRACT *(Continue on reverse side if necessary and identify by block number)*

This work is aimed at understanding the origin of fatigue enhanced photo-stimulated exo-electron emission. The experimental part thereof is reported in the bulk of this report and the theoretical analysis in the Appendix of the report.

Measurements of the photoyield of flexurally fatigued aluminum are reported as a function of photon energy for several different initial microstructures →

DD FORM 1 JAN 73 1473 EDITION OF 1 NOV 65 IS OBSOLETE

389 949

UNCLASSIFIED

SECURITY CLASSIFICATION OF THIS PAGE *(When Data Entered)*

of the material; samples were prepared under well-annealed and work hardened conditions, and some were doped with small copper additions. It was found that for photon energies less than about 9 eV fatigue enhances the photoemission. It was also observed that this "photo-stimulated exo-electron emission" is quite sensitive to the initial microstructure. The enhancement occurs much more rapidly with fatigue for well-annealed Al than for work hardened specimens. The results appear to be consistent with a model, presented in the Appendix, which is based on a resonant coupling between the surface electromagnetic modes (plasmons) of the metal and the incident photons. This resonance is made possible by the development of dislocation slip steps on the surface during fatigue. The effect of material condition is shown to be primarily a difference in the kinetics of slip step formation. The effects of ion sputtering to remove oxides and of the angle of incidence of the photons are also reported. Above 9 eV the photoyield was found to be almost insensitive to fatigue. Possibilities to use the "photo-stimulated exo-electron emission" as a fatigue detector are briefly discussed.

TABLE OF CONTENTS

		Page
REPORT DOCUMENTATION PAGE		
1.0	INTRODUCTION	1
2.0	EXPERIMENTAL	4
3.0	RESULTS	6
	3.1 Photoyield of Commercially Pure Aluminum Al 1100	6
	3.2 Effects of Shot-Peening on Y(Al)	8
	3.3 Effects of Surface Slip on Y(Al)	9
	3.4 Effects of Fatigue Hardening and Softening on Y(Al)	9
	3.5 Photoyield of an Aluminum Single Crystal	10
	3.6 Photoyield of Copper Doped Aluminum	11
	3.7 Photoyield of Nickel and Titanium	12
4.0	DISCUSSION OF EXPERIMENTAL RESULTS	14
5.0	SUMMARY AND CONCLUSIONS	19
6.0	ACKNOWLEDGEMENTS	21
7.0	REFERENCES	22
8.0	BIBLIOGRAPHY	24
	8.1 Previous Reports Resulting from Contract No. F44620-71-C-0043	24
	8.2 Publications Resulting from Contract No. F44620-71-C-0043	24
APPENDIX	- THE THEORETICAL BASIS FOR EXO-ELECTRON EMISSION (ROUGHNESS INDUCED PHOTOEMISSION)	A1
REFERENCES - APPENDIX		A14

TABLE OF CONTENTS - (Continued)

Page

LIST OF FIGURES

Fig. 1 Surface replica of Al 1100 (HO) after 4000 cycles, showing a dense slipline pattern 26

Fig. 2 Schematic diagram of ultra-high vacuum system to determine fatigue enhanced photoemission 27

Fig. 3 View of installed specimen 28

Fig. 4 Photoyield of gold as a function of incident photon energy 29

Fig. 5 Photoyield of etched Al 1100 (H14) as a function of incident energy and fatigue 30

Fig. 6 Photoyield of etched and ion sputtered Al 1100 (H14) as a function of incident energy and fatigue 31

Fig. 7 Photoyield of etched Al 1100 (HO) as a function of incident energy and fatigue 32

Fig. 8 Photoyield of ion sputtered Al 1100 (HO) as a function of incident energy and fatigue 33

Fig. 9 Photoyield of Al 1100 (HO and H14) as a function of fatigue (at 7.3 eV) 34

Fig. 10 Photoyield of ion sputtered Al 1100 (H14) as a function of oxide redeposition 35

Fig. 11 Photoyield of ion sputtered Al 1100 (H14) as a function of oxide redeposition 36

Fig. 12 The relative change of the photoyield as a function of fatigue and cycle of incidence of photons (at 7.8 eV) . . . 37

Fig. 13 Comparison of surface roughness due to shot-peening with Al_2O_3 particles prior to fatigue (SEM) 38

Fig. 14 Photoyield of shot-peened (10μm Al_2O_3 particles) and etched Al 1100 (HO) as a function of incident energy and fatigue. . 39

Fig. 15 Photoyield of shot-peened and etched (50μm Al_2O_3 particles) Al 1100 (HO) as a function of incident energy and fatigue. . 40

Fig. 16 Photoyield of Al 1100 (HO) after different degrees of shot-peening as a function of fatigue (at 7.3 eV) 41

TABLE OF CONTENTS - (Continued)

Page

Fig. 17 Development of surface slip on Al 1100 (HO) as a function of fatigue (optical micrographs of etched surfaces) 42

Fig. 18 The change of photoyield (at 7.3 eV) with surface area covered by slip. Material: Al 1100 HO 43

Fig. 19 Slip line traces at different states of fatigue (surface replicas) 44

Fig. 20 Comparison of the Knoop hardness, K.H., for Al 1100 HO and Al 1100 H14 as a function of fatigue 45

Fig. 21 X-ray Laue pattern and slip line development on Al single crystal 46

Fig. 22 Photoyield of Al single crystal compared with Al 1100 HO 47

Fig. 23 Photoyield of etched Al 1%Cu as a function of incident energy and fatigue 48

Fig. 24 Photoyield of etched Al 3%Cu as a function of incident energy and fatigue 49

Fig. 25 Photoyield of Al 0%Cu, Al 1%Cu and Al 3%Cu compared with Al 1100 HO (prior to fatigue) 50

Fig. 26 Slip line traces developed after 4000 cycles of fatigue (failure) of Al 1%Cu 51

Fig. 27 Surface replica of Al 1%Cu fatigued for 250 cycles 52

Fig. 28 Photoyield of etched titanium as a function of incident energy and fatigue 53

Fig. 29 Photoyield of ion sputtered and etched nickel as a function of incident energy and fatigue 54

Fig. 30 Surface replica of Al 2219 T851, showing a crack initiated at an intermetallic. Slip line development indicated by arrow 55

Fig. A1 Diagram of the coordinate system illustrating the sinusoidal roughness at the metal-oxide interface A15

Fig. A2 Illustration of the symmetry condition on the electron current diffracted by the picket fence in the equivalent infinite medium, $J_x(z) = J_x(-z)$, $J_z(-z) = -J_z(z)$ A16

TABLE OF CONTENTS - (Continued)

Page

Fig. A3 Integration contour used to invert the Fourier sums in the variable conjugate to z A17

Fig. A4 Energy dispersion curves of the surface plasmon with weak periodic coupling (periodic coupling only qualitative) of spacing d = 1/16 μm. The straight line is the dispersion curve for light incident at 60° from normal. If that light is polarized in x-z plane, resonant absorption occurs where the light line intersects the plasmon dispersion curve A18

Fig. A5 The change in photoyield of Al 1100 HO, normalized by the calculated photoyield in metal (oxide layer 120Å thick). Data calculated using raw data shown in Fig. 7 of the report A19

Fig. A6 Theoretical prediction of absorption of aluminum with periodically oscillating surface of amplitude 15A and period 625A and with an oxide layer 120Å thick for P polarized light incident at 60° from the normal. The dashed curve is the absorption with the surface oscillation assumed to be only 1A, and is indistinguishable from that of a flat surface. This calculation retained only the first resonance; retention of additional terms would produce a second peak about 1 eV higher in photon energy A20

1.0 INTRODUCTION

Mechanical deformation of a metal produces electron emission, usually called exo-electron emission,[1] via (at least) three different mechanisms: "tribostimulated" exo-electron emission involving electrons ejected during the deformation, thermally stimulated exo-electron emission, and photo-stimulated exo-electron emission. The tribostimulated exo-electrons have been shown[2] to result from brittle fracture of the surface oxide. Although no single mechanism has been established for thermally stimulated exo-electron emission, it, too, exists only when an oxide is damaged.[3] These are both "transient" phenomena; continued stimulation eventually removes all of the exo-electrons from a particular "event." The ultraviolet photoemission, in contrast, is caused by deformation and persists as long as deformation and bright illumination are continued. The deformation produces a change in the number of electrons per incident photon, and a constant current will result from constant illumination. This program deals only with deformation enhanced ultraviolet (photon energy greater than the work function) photoemission, and, more specifically, only with that portion which can persist even after the re-oxidation of a fresh surface. The characteristics just described provide this effect with distinct advantages as a materials science and non-destructive testing tool. There is a large body of literature describing the transient phenomena,[4-18] but relatively little attention has been given to this apparently more useful mechanism until recently.[19-21]

During the past few years there has been substantial basic research on the effect of surface roughness on the UV photoyield from clean metals.[20-26] Small deviations from a perfectly flat surface permit the incident electromagnetic wave to excite a surface charge oscillation of the electron gas. This increases the absorption of light and ultimately the photoyield. It should be emphasized that this roughness enhanced photoemission is not only due to the exposure of fresh metal by cracking of the brittle oxide, but exists even for an oxide-free surface in high vacuum. Baxter[27] has shown that the cracking of the oxide results in a very large localized increase in the photoyield, and found that, although the spatially localized photoemission disappeared with re-oxidation, the average photoyield

remained far above the pre-fatigue background. Moreover, it has been shown[19] that fatigue enhances photoemission even when the surface is oxide free. This was established by ion sputtering the sample to remove the oxide, and then fatiguing in a vacuum. This inexhaustible photostimulated exo-electron emission is the subject of this investigation. Since fatigue increases the surface roughness of a material, it is natural to speculate that the roughness enhanced coupling is the underlying mechanism. It should be noted, however, that the rms roughness of an unfatigued specimen in our experiments is probably an order of magnitude greater than the roughest specimen of Endriz and Spicer,[22] and that the changes in the initial stages of fatigue are small, typically a few Burgers vectors. The experiments reported here are intended to test this conjecture, and, more generally, to determine the importance (if any) of the wavelength and angle of incidence of the light, and of previous internal deformation.

The photoyield from both well-annealed and work-hardened commercially pure aluminum samples, fatigued in flexure, was determined.[20] As a consequence of a difference in the initial dislocation density and substructure in these two states, it would be expected that the developed surface roughness (an example of which is shown in Fig. 1) will be different in each case, and thus it is of scientific and practical interest to test whether the exo-electron emission can distinguish such details of the materials condition. Ion sputtering to remove surface oxides was also employed in the present experiments. Furthermore, the fatigue enhanced photoemission from aluminum was measured for light incident at different angles. Most of these results have been reported in last year's Interim Report[28] as well as in the open literature[20] and will thus be discussed only briefly in the present Final Report.

Over the past several months extensive measurements on the effects of shot-peening on subsequent fatigue enhanced photoemission and on the effects of alloying additions (copper) on this process have been performed. In the latter experiments it was observed that the slip mode

character is quite different from that found on the commercially pure samples, due to grain growth during the annealing treatment. Grain diameters of 1-2 μm have been obtained with pronounced banded slip. Despite this unexpected deformation behavior, an increase of the photoyield was observed. Additional photoemission work was done on an oriented aluminum single crystal and results obtained were in agreement with the postulated roughness induced coupling model, outlined below.

The theory of deformation enhanced photoemission given in the Appendix to this report is based upon the experimental observation that plastic deformation produces a weak, nearly periodic modulation of the metal surface. This is shown in the electron microscope picture (Fig. 1) of Al 1100 at 10% of its fatigue life. The photoyield from 1800Å light is increased by about 40% above that from the unfatigued surface. The theory, sponsored by Rockwell International IR&D funds, shows that such a weak, periodic modulation of a metal surface produces resonant absorption of light by surface electromagnetic waves (surface plasmons). These collective excitations of the conduction electrons can decay to a single electron excitation, which allows electrons to escape from the metal if the surface plasmon energy exceeds the work function. The absence of a significant effect in some metals, like titanium,[28] is probably because the surface plasmon energy is comparable to or less than the work function. The material properties which determine the characteristics of the plasmon coupling are the dielectric properties of the metal and its surface oxide, the work function, and the metallurgical variables which determine the nature of the slip step formation. Also given in the Appendix is a brief description of the coupling to the surface plasmon by a weak periodic modulation of the metal surface. This leads to predictions about the wavelength, angle of incidence, and polarization dependence of this coupling. A brief outline of this theory will be published in the open literature[29] and in full detail in Ref. 30.

2.0 EXPERIMENTAL

The experiments were performed in an ultra-high vacuum chamber at a base pressure of 5×10^{-8} torr (see Fig. 2). The major residual gasses in the chamber were determined to be H_2, H_2O, and CO by means of a quadrupole mass spectrometer attached to the chamber. The material used for most of the experiments was commercially pure Al 1100 in the well-annealed (H0) or work hardened state (H14). Further experiments were performed on material prepared by the Science Center, an aluminum single crystal and polycrystalline aluminum (99.999%), doped with 1% and 3% copper, respectively. The doped material was annealed after sample preparation at 500° C for about 1 hr. Additional experiments were performed on a titanium and a nickel specimen. All specimens were of the cantilever beam type and were flexurally fatigued in situ as shown in Fig. 3. They were tapered in width so that a homogeneous strain (or stress) over their length was achieved (strain amplitude for all specimens $\varepsilon_{max} \approx 3 \times 10^{-3}$). The sample surfaces were electropolished and then chemically etched immediately prior to placement in the vacuum apparatus. This procedure resulted in approximately a 120Å thick oxide layer on the Al, as determined by sputtering with argon ions and taking a depth profile using Auger electron spectroscopy, as well as by ellipsometric studies outside the above chamber. This procedure was also used to obtain relatively thin oxide layers of about 15-20Å, the results of which will be reported in the following. It was impossible to determine with certainty whether or not this thin oxide grows appreciably during the time it takes to fatigue the specimens to failure, although some indirect indication exists that the oxide did not regrow.

The variable wavelength photon source used was a McPherson 0.3 meter monochromator equipped with an arc lamp in which H_2 was the working gas (see Fig. 2). This provided useable light with wavelengths ranging from about 1100Å to about 2200Å, corresponding to photon energies from 11.3 to 5.6 eV over a spot size of about 2 x 2 mm. The photocurrent was measured by means of a picoammeter connected between the sample and ground, and the light was incident upon the sample at an angle of 60° from normal, unless specified otherwise. To calibrate the photocurrent of Al in photoyield,

the specimen was replaced by a gold sample with known photoyield.[31] Since the photoyield in the original work[31] is given in electrons/absorbed photon, a correction factor (1 - R) was applied (R = reflectivity) to convert the data to electrons/incident photon (Y(AU)) which is plotted in Fig. 4. The system also contained an argon ion bombarded gun used for sample cleaning and a grazing incidence electron gun used to excite Auger transitions to monitor the surface chemistry of the sample (see Fig. 2). It was also attempted to obtain an analysis of the emitted electron energy using a retarding grid system. This analyzer (see also Fig. 2) is a converted 4 grid LEED optics with the sample, first grid and fourth grid grounded. The energy resolution of the system is enhanced by the additional inclusion of a post monochrometer. Energy distribution curves were obtained by imposing a negative ramp voltage modulated by a small AC voltage upon the second-third grid combination, and by using standard phase sensitive detection techniques, the output from the electron multiplier (which is at the same frequency as the grid modulation) could be detected. Some of the results on such an analysis have been reported in Ref. 28. Some later measurements on a platinum specimen, however, have cast some doubts on the validity of these measurements, in that the energy distribution unexpectedly was quite similar to the ones reported in Ref. 28. Definitely, more work has to be done to be sure that only electrons from the aluminum are analyzed and nothing else, as is suspected at the present.

3.0 RESULTS

3.1 Photoyield of Commercially Pure Aluminum Al 1100. Photoyield Y(Al) curves on aluminum were taken as a function of: (1) the number of fatigue cycles, (2) the incident photon energy, (3) the initial state of deformation (in two conditions, HO and H14), (4) the oxide thickness, and (5) the angle of incidence of the stimulating photons. Examples of some of the results are shown in Figs. 5-8. At least two pronounced effects can be seen. They are: (1) In general, fatigue increases Y(Al) over the pre-fatigued value (at least up to about 9 eV), as seen in Figs. 5 and 7, and (2) Ion sputtering prior to fatigue enhances the photoyield by about a factor of three over that of non-sputtered materials, as seen in Fig. 6. The first few hundred fatigue cycles after ion sputtering reduce Y(Al) by about 20% for both materials (an example of which is shown in Fig. 8). Thereafter the fatigue enhanced photoyield changes in the same fashion as it did without prior ion sputtering (at a higher level though, indicating that no re-oxidation occurred). The effect of fatigue on Y(Al) is more complicated at incident energies above about 9 eV. In most cases it was observed that the yield decreased slightly with increasing fatigue. As will be discussed in detail in a forthcoming publication,[30] the photoyield in this energy range (above 9 eV) is dominated by the oxide on the surface. In this region the photocurrent to ground may contain a spurious component due to oxide charging.

A cross-plot of the photoyield Y(Al) as a function of the number of fatigue cycles at an incident energy of 7.3 eV is shown in Fig. 9. This is a typical example of the change of the photoyield with fatigue for incident energies in the range of 5.9 up to about 9 eV. The differences between the two materials' conditions (H14 versus HO) and the surface treatments (etched versus ion sputtered) are quite obvious. Changes of Y(Al) with fatigue are more pronounced in the well-annealed (HO) material with a maximum in Y(Al) occurring at about 20,000 cycles ($\approx$ 50% fatigue life) and the maximum change occurring between 0 and 10,000 fatigue cycles. This initial change is about a factor of six larger than the one observed on the work-hardened (H14) materials. The authors believe that the large increase in Y(Al) during the early fatigue stage of the HO material is caused by the pronounced slip-step formation on the surface of this material (see Fig. 1). Both

phenomena are less pronounced on the H14 material, as may be seen from Fig. 9. When the surface is completely filled with these slip-steps no further increase in the photoyield from the HO material is observed.[20]

Since it is known that ion sputtering leads not only to a reduction of the surface oxide layer, but also to a fair amount of radiation damage and surface roughness different from the fatigue induced roughness, an annealing experiment after sputtering was performed with the expectation that any roughness contributed to Y(Al) would be eliminated by a smoothing of the surface through a diffusion process. The results are shown in Fig. 10. Although the ion sputtering enhancement of Y(Al) was not as large as expected from the previous results, a 300°C anneal (temperature achieved by electron bombarding the specimen on the side opposite to the photo-stimulated one) caused a reduction of the photoyield. The first 100 fatigue cycles decreased Y(Al) even further before onset of the fatigue enhancement of Y(Al) (250 cycles). Although further experiments (e.g., annealing before ion sputtering) are necessary, the present results indicate that ion sputtering induced disorder on the surface enhances the photoyield. In addition, the reduction of the oxide layer thickness will enhance the photoyield. To show this effect the photoyield of an ion sputtered specimen was measured as a function of exposure to air (exposures: 3×10^2 Langmuirs and 3×10^4 Langmuirs, with the latter giving an oxide layer thickness comparable to that obtained by etching). Figure 11 shows the decrease of Y(Al) with oxide formation, which is less than the enhancement obtained during sputtering.

All results described so far were obtained using light incident at an angle of 60° with respect to the surface normal. To study the effects of the angle of incidence on photostimulated exo-electron emission, an experiment was performed on etched HO material. The results at 7.3 eV, shown in Fig. 12, were normalized at zero fatigue to compare the effects of the fatigue enhancement at several angles of incidence. In relatively good agreement with earlier results,[20] obtained on an ion-sputtered specimen, it is observed that Y(Al) is more enhanced for shallow angles of incidence (at least up to 60°). Such a trend is to be expected qualitatively if Y(Al) is caused by surface plasmons, since the coupling is less efficient at steeper angles of incidence.

Since the major emphasis of this paper is fatigue enhanced photoemission, and since the photoemission is strongly fatigue-dependent only in the early stages of fatigue life, observations on the roughness induced by fatigue were concentrated on these early stages. As was reported earlier,[20] results obtained by a surface replication technique show that after about 10% of the fatigue life (about 4000 fatigue cycles) the material in the H14 condition (work-hardened) shows small signs of slip-step formation; in contrast, these features are very pronounced on the material in the HO condition (well-annealed) at this point in the life of the specimen (Fig. 1). For both materials the slip-steps lead to intrusions-extrusions and finally microcracks which can be observed after about 10,000 fatigue cycles. Using the scanning electron microscope, microcrack densities are about the same for both materials at that point in life. However, the overall surface roughness of the two materials is markedly different for the two materials.[20] In the H14 condition the surface shows almost featureless "mesas" (about 200-300μ wide) interrupted by microcracks. In the HO condition the surface topography consists of a long wavelength, high amplitude undulation (wavelength about 200μ) with microcracks in the valleys of this undulation. Thus, microcrack densities are about the same for both materials' conditions.

3.2 Effects of Shot-Peening on Y(Al). Stimulated by the ion sputtering results, fatigue enhanced photoemission was measured after shot-peening the surface of Al 1100 HO with Al_2O_3 particles of 10 μm and 50 μm diameter. After shot-peening the specimens were annealed, to reinstate the HO condition, and etched. Scanning electron microscope pictures of the specimens prior to fatigue, in comparison to the etched-only surface, are shown in Fig. 13. Photoyield as a function of incident energy and fatigue was then obtained, as shown in Figs. 14 and 15. The results at 7.3 eV, versus the number of fatigue cycles applied, are shown in Fig. 16. As expected, shot-peening increased the photoyield prior to fatigue. The photoyield following shot-peening increased with fatigue almost independently of prior roughness, similarly to that observed after ion sputtering. In the present experiments the large initial decrease in Y(Al) during the first few hundred fatigue cycles was not observed, however. This is probably caused by the annealing treatment after shot-peening.

3.3 Effects of Surface Slip on Y(Al). To further study and substantiate the effects of surface slip steps on Y(Al), a series of experiments was performed in which Al 1100 HO specimens were studied at different levels of fatigue. Figure 17 shows the development of surface slip using optical microscopy on etched specimens as they are used for the actual photoyield measurements. As may be seen from this figure the slip develops in patches which grow as fatigue proceeds. In Fig. 18 the photoyield increase $\Delta Y(Al)$ at 7.3 eV is plotted against the surface area covered with slip, as estimated from Fig. 17. These two quantities apparently obey a linear relationship. Since fine details of individual slip steps cannot be resolved from etched surfaces, electropolished Al 1100 HO specimens were fatigued to the same levels as shown in Fig. 17. The results of surface replicas taken from the electropolished specimens are shown in Fig. 19. Comparison of these replicas from different states of fatigue indicates qualitatively that the periodicity of the slip steps is not a function of fatigue (at least for Al 1100 HO). Thus it is concluded that the fine structure of the fatigue enhanced roughness does not appreciably change as a function of fatigue; however, the total surface area covered by this fine structure increases about linearly with the number of fatigue cycles applied to the specimen.

3.4 Effects of Fatigue Hardening and Softening on Y(Al). Since the major emphasis of this program is fatigue enhanced photoemission, and since the photoemission is strongly fatigue-dependent only in the early stages of fatigue life (see Fig. 9), observations on the roughness induced by fatigue were concentrated on these early stages. As discussed in an earlier paper[20] the material in the H14 condition (work-hardened) shows only little signs of slip-step formation after about 10% of the total fatigue life has passed. In contrast, slip-step formation is very pronounced on the material in the HO condition (well-annealed) at this point in the life of the specimen (see Fig. 1). Likewise, changes of Y(Al) with fatigue are more pronounced in the well-annealed (HO) material with a maximum in Y(Al) occurring at about 20,000 cycles ($\approx$ 50% fatigue life). As pointed out before, the initial change of Y(Al) with fatigue is about a factor of six larger for the HO material than observed on the H14 material.

The topographical changes on the surface of these materials are fairly well understood from observations on the fatigue behavior of the materials. As pointed out by Grosskreutz,[32,33] the well-annealed (HO) material should harden in the early stages of fatigue since increases in the dislocation density in the bulk of the material are accompanied by pronounced slip-step formation at the surface. In contrast, the material which is in an initially work hardened state (H14) should soften, since the initially complex dislocation arrangement breaks up into a cell structure. Slip-step formation is much less pronounced at the surface since dislocation motion is restricted by the high dislocation density. To demonstrate the applicability of the model to the present case, the surface hardness of HO and H14 materials was determined as a function of fatigue. These results are plotted in Fig. 20 with the surface hardness measured by a Knoop hardness (K.H.) indenter. As may be seen, the trends in K.H. with fatigue for both materials are as expected. Since in one case the surface hardness decreases with fatigue (H14), and in the other case increases (HO), with the photoyield, Y(Al), increasing in both cases (see Fig. 9), it is concluded that Y(Al) is not a unique function of surface hardness, K.H. Furthermore, since K.H. depended on the dislocation structure close to the surface and thus to the microscopic internal stresses (for a definition of internal stresses see Ref. 34), Y(Al) is not found to be a unique function of these microscopic internal stresses.

3.5 Photoyield of an Aluminum Single Crystal. With the previous results in mind, an experiment on the change of the photoyield of an aluminum single crystal was performed. It was hoped that by using a single crystal, coverage by slip lines over the entire surface should occur within the first few fatigue cycles and the photoyield should thus increase very strongly.

The single crystal was chosen such that the specimen's surface was a (100) plane. Within this plane the specimen was oriented such that the maximum stress during fatigue was perpendicular to one of the traces of a (111) plane intersecting the (100) surface. Thus only single slip should occur. Figure 21, top, shows the x-ray Laue pattern of this single crystal,

with the slip traces resulting from 100 cycles of fatigue shown at the bottom of this figure. Indeed, only single slip occurred. However, in contrast to the expectations, the slip is heavily banded. The photoyield results are shown in Fig. 22. Two surprising results were obtained: (1) The photoyield of the virgin single crystal (0 fatigue cycles) is markedly different from that of an Al 1100 HO specimen (dashed line in Fig. 22). (2) The photoyield of the single crystal did not show the expected large increase. The first result cannot be explained at the present time. However, in the following section similar results on Science Center-prepared materials will be discussed. Result (2), however, is easily understood in terms of the plasmon model. After receiving the experimental arrangement, it was noted that the stimulating light was incident in the direction of the slip steps formed during fatigue. Thus a component which could excite plasmon oscillations was not present. The present experimental setup, unfortunately, did not allow a rotation of the specimen around the normal to the surface to prove our conjecture fully.

3.6 Photoyield of Copper Doped Aluminum. In an attempt to determine the effects of fatigue on the photoyield of copper doped aluminum, three alloys were prepared; Al 0%Cu, Al 1%Cu, and Al 3%Cu, which were annealed at 500°C for 1 hr. Copper additions effectively raise the yield stress of aluminum and, at the same time, should change the homogeneous slip of the Al 1100 HO (see Fig. 1) to a more coarse slip mode pattern. To a certain degree, the Al 3%Cu is thought to be a model system for the 2000 series aluminum alloys (which contain about 4% Cu); however, the intermetallic particles, usually found in the 2000 series aluminum,[35] are not present in the Science Center-prepared materials (intermetallics are preferential crack initiation sites in high strength aluminum alloys[35]). Results of the fatigue enhancement of the photoyield for the two copper doped model alloys are shown in Figs. 23 and 24. Total fatigue life of these alloys was relatively short; both specimens failed between 4000 and 4500 cycles (at $\varepsilon_{max} \approx 3 \times 10^{-3}$). Both specimens showed surprisingly large photoyield increases with the major change occurring between 0 and 100 fatigue cycles.

Unexpectedly, the third specimen (Al 0%Cu) did not show any signs of fatigue enhanced photoemission. A comparison of the photoyield of the three alloys with the one obtained on Al 1100 HO is shown in Fig. 25 of Y(Al) of the Science Center-prepared alloys prior to fatigue (0 fatigue cycles) is quite different from that of an Al 1100 HO specimen (dashed line in Fig. 25). This shape change appears not to be a consequence of the copper additions.

The relatively large change of the photoyield after the first 100 fatigue cycles as observed on Al 1%Cu and Al 3%Cu, and the total absence of a change on Al 0%Cu is surprising. Optical microscopy revealed that the grain diameter of these specimens was quite large (1-2 mm diameter). Grains oriented unfavorably with respect to the major stress axis did not show any slip step formation. This may account for the absence of a fatigue enhanced emission from the Al 0%Cu specimen: If the stimulating light spot (about 2 mm diameter) hit such a grain, one should not expect an effect. On the other hand, the strong effects after 100 fatigue cycles observed on Al 1%Cu and Al 3%Cu are in agreement with our expectations. Figure 26, an example of banded slip on the surface of the Al 1%Cu after the specimen failed at about 4000 cycles, indicates the large grain size of the material. This slip band formation occurred early in the fatigue life.

3.7 Photoyield of Nickel and Titanium. Some measurements of the photoyield of commercially pure nickel and α-titanium specimens were made as a function of fatigue and photon energy.[28] Well annealed α-titanium shows very pronounced effects of fatigue on photoyield below about 7.5 eV (as shown in Fig. 28). As in the case of HO (well annealed) aluminum, Y increases initially with fatigue. Maximum photoyield occurs at about 500 cycles. Thereafter the photoyield decreases again. This is not a surprising result since α-titanium (hexagonal structure) shows very pronounced single slip, similar to aluminum, at the beginning of the fatigue. In contrast, very little effect of fatigue on photoyield of nickel was observed. Since the first work hardened specimen (Ni etched) did not show systematic effects (see Fig. 20), another specimen was annealed and ion sputtered before fatigue (Ni ion sputtered). Again no systematic

effects were observed (see Fig. 29 also), although the photoyield was generally much larger for this specimen than for the first one.

4.0 DISCUSSION OF EXPERIMENTAL RESULTS

The present discussion will be mainly concerned with a qualitative comparison of the photoyield results and the topographical surface features as presented in the previous section. The details of the mechanisms for the fatigue enhanced photoemission will be discussed in the Appendix of this report which deals with the mechanism of surface charge oscillations.

The cross-plot of the photoyield Y(Al) as a function of fatigue cycles at an incident energy of 7.3 eV, as shown in Fig. 9, is a typical example of the change of the photoyield with fatigue for incident energies in the range of 5.9 up to about 9 eV. The differences between the two materials' conditions (H14 versus HO) and the surface treatments (etched versus ion sputtered) are quite obvious. Changes of Y(Al) with fatigue are more pronounced in the well-annealed (HO) material with a maximum in Y(Al) occurring at about 20,000 cycles ($\approx$ 50% fatigue life) and the maximum change occurring between 0 and 10,000 fatigue cycles. This initial change is about a factor of six larger than the one observed on the work-hardened (H14) materials. The measurements suggest that the large increase in Y(Al) during the early fatigue stage of the HO material is caused by the pronounced slip-step formation on the surface of this material (see Fig. 1) and that the fatigue enhanced photoyield increases about linearly with the surface area covered by these steps (Fig. 18). The effect is less pronounced on the H14 material. When the surface is completely filled with these slip-steps no further increase in the photoyield from the HO material is observed. Since microcracks are being formed at this point in the specimen's fatigue life, the results on the HO material seem to indicate that the microcracks themselves do not significantly affect the yield.

The topographical changes on the surface of these materials are fairly well understood from observations on the fatigue behavior of the materials.[20,30] The well-annealed material will harden in the early stages of fatigue as the dislocation density in the bulk of the material increases, accompanied by pronounced slip-step formation at the surface. Eventually the dislocations form a cell structure with individual dislocations of long loop length shuttling to and fro between the cell walls. At the surface this process leads to microcrack formation. This latter part of the fatigue life usually

is referred to as the saturation stage of fatigue. In contrast, a material which is initially in a work hardened state (H14) condition behaves differently, at least during the initial stages of fatigue.[32,33] The material will soften as the initial complex dislocation structure breaks up into a cell structure. Slip-step formation is much less pronounced at the surface since dislocation motion is restricted due to the high dislocation density. Once the cells have been formed, microcrack formation in the saturation stage will occur similarly to that outlined above for the HO material. The fatigue model thus accounts qualitatively for the observed changes in Y(Al) with fatigue through the differences in the slip line patterns due to the dislocation motion in the vicinity of the surface.

It should also be noted that the initial surface etch leads to an almost identical Y(Al) of about 2.5×10^{-4} electrons/incident photon for both materials, demonstrating that surface preparation by etching leads to reproducible results. Ion sputtering leads to about a threefold increase of Y(Al) over the yield obtained by etching (see Fig. 9). As was mentioned before it is believed that this increase is a combined effect of oxide removal and generation of surface roughness due to sputtering. The decrease of Y(Al) during the first ?% of the fatigue life suggests strongly that the fatigue enhanced roughening eliminates some fraction of the sputtering induced roughening.

The annealing experiments after ion sputtering (Fig. 6) were designed to determine the extent to which the sputtering induced roughness enhanced the photoyield. At 7.3 eV these experiments indicate a reduction of the yield from 4×10^{-4} to 2×10^{-4} electrons per incident photon due to surface diffusion and smoothing of the surface. This difference is about the same as that obtained during the initial stages of fatigue of the sputtered samples. Therefore, it appears that the total sputtering induced roughening is eliminated by the fatigue. The remainder of the sputtering enhanced photoyield, roughly 4×10^{-4} electrons per incident photon, should then be caused by the almost complete elimination of the oxide. This is in agreement with the reoxidation experiment at 7.3 eV, shown in Fig. 11, indicating a yield reduction of about 4×10^{-4} electrons per incident photon after an exposure to 3×10^{4} Langmuir. Thus a fairly consistent set of data on the effects of a roughly 120Å thick oxide layer and ion sputtering

induced roughness on the photoyield at 7.3 eV has been obtained. It should be kept in mind, however, that the absolute values quoted above will strongly depend on the angle of incidence of the stimulating light, as shown in Fig. 12.

From a practical point of view the results of the shot-peening experiments (Figs. 13-15) seem to be very interesting, in that they indicate that the fatigue enhanced photoyield is independent of surface roughness prior to fatigue (in agreement with ion-sputtering experiments). The present authors believe that these results are of some importance for application of the photoyield as a fatigue detector. Most metallic surfaces show relatively large roughness due to machining. Such roughness may not interfere with the fatigue induced roughness; however, it is definitely a quantity superimposed (as a bias) on the fatigue induced roughness. Both fatigue hardening and softening increase the fatigue enhanced photoyield, as was demonstrated by determination of the Knoop hardness of the material. It can thus be concluded that the photoyield is not a unique function of these internal stresses; however, the photoyield increases as long as the state of the microscopic internal stresses changes. Again, this is of some practical importance in that, if dislocation motion is the micromechanism for fatigue, only the earlier parts of the total fatigue life give rise to photoemission. In high strength aluminum alloys, the fatigue is determined by microcrack growth starting at intermetallic inclusions.[35] As was pointed out earlier, microcracks as such should not give rise to photoemission. It was thus decided to use surface replication to investigate whether or not these microcracks would produce a "plastic zone" indicated by slip-step formation at the surface. Preliminary results (an example of which is given in Fig. 30) indeed show such slip traces, probably giving rise to the photoemission in the vicinity of a crack tip, observed by Baxter and Rouze[36] using an "Exo-Electron Microscope."

Due to the similar slip patterns observed on the Al single crystal and the Al-Cu alloys, it is most convenient to discuss these results together. In either case, the slip observed was heavily banded, which was quite unexpected for the single crystal. It is speculated at the present time that the banded slip is a consequence of the large grain size.

In case of the Al 1100 specimens, with a small grain size, mobilization of dislocation sources in the vicinity of the grain boundaries are probably the cause of slip step formation. Since the grains are small, there is little hardening which would stop further dislocation mobilization (as may be the case for large diameter grains). The different shape of the photoyield versus incident energy for the Science Center-prepared materials with respect to the commercial Al 1100 materials, cannot be explained at the present time. However, it appears that even banded slip causes a fatigue enhanced photoyield. As expected, the major change of Y(Al) occurs in the very early stages of fatigue (at least for the Al-Cu alloys). The absence of the effect during fatigue of the single crystal may be explained by the fact that the wave vector of the light did not contain a component which is able to simulate the photoyield.

In conclusion, the present results are, in general, in good agreement with the ones presented by Baxter and Rouze[21,27,36] and Thompson, et al.[19] As has been shown by these authors, a fresh, oxide-free surface will be a more efficient electron emitter than an oxide covered surface. If the breakup of the oxide layer by fatigue was the principal source of fatigue-enhanced photoemission, no fatigue enhancement of the photoyield should occur from an ion-sputtered surface. The present results, as well as the data presented by Thompson, et al.[19] demonstrate that this is not the case; the change of Y(Al) during fatigue is roughly independent of the thickness of the surface oxide layer. It is this fatigue enhanced emission which will be discussed in the Appendix to this report. In particular it will be shown that the change in yield as a function of the stimulating frequency is in relative good agreement with the notion of a roughness induced coupling of the incident photon to the surface plasmon oscillation, the decay of which ejects the electrons.

It is interesting to note, again, that the present data indicate that roughness enhanced electron emission from commercial Al alloys is mainly caused by slip-step formation at the free surface of the plastic zone ahead of microcracks (or a macrocrack). The fatigue mechanism of such alloys is, however, quite different from the ones discussed in the present paper. Such alloys contain small intermetallics at which microcracks

start to grow into the matrix.[35] Since the dislocation motion in the plastic zone is rather restricted (similar to Al 1100 H14), it is expected that the Y(Al)-fatigue life curves will be similar to the present H14 results. Indeed, comparison of results on Al 2024-T3[19] with the present H14 results support this conjecture.

5.0 SUMMARY AND CONCLUSIONS

The principal conclusion from this work is that slip steps are a source of fatigue enhanced photoemission, and if the experiment eliminates the highly localized enhancement due to exposure of bare metal (for example, by exposing the sample to oxygen), the formation of slip steps is the only source of the fatigue enhancement. The enhancement of the photoyield is proportional to the area covered by slip steps, and thus measures the extent of plastic deformation. The detailed physical mechanism proposed in the Appendix (the resonant coupling of the incident light to surface charge oscillations) is supported by this rather broad range of experimental observations, although certain additional tests are desirable. Practically speaking, the observations on angular dependence, wavelength dependence, roughening prior to fatigue, and material condition are a necessary basis for development of photostimulated exo-electron emission for fatigue or deformation monitoring. The theory given in the Appendix provides a quantitative guide to extrapolation to materials other than those discussed here. A beautiful application of the roughness induced photoemission to fatigue crack propagation was described recently by Baxter and Rouze,[36] who used an incident energy of about 5 eV. In contrast to the present technique, which looks at the effect integrated over the total surface, their method, using the optics of an electron microscope, looks at the effect locally. This latter method, therefore, is able to detect load "hot spots"; e.g., areas where plastic deformation occurs. It is thus well suited, in some version or another, to be used as a fatigue monitoring system. The present experiments show that the instrument's sensitivity to fatigue enhanced emission could be increased if a stimulating energy in the neighborhood of 7 eV is used (at least in the case of aluminum!). Unfortunately, there seem to be no laser systems available at the present time which produce such a high energy. However, 5 eV (a system as used by Baxter and Rouze[36]) should be enough to observe an effect on photoyield.

Furthermore, the present studies indicate that it is not necessary to employ a vacuum to study fatigue enhanced emission, although the oxide acts as an attenuator. Using enough intensity should allow

observation of the roughness induced emission, as was indeed observed in earlier work.[37] Particularly interesting from a practical point of view are the present observations that surface roughness, induced prior to fatigue (by shot-peening in the present case), does not interfere with the fatigue enhanced emission. Most surfaces in a practical situation definitely show a certain roughness component (due to machining, etc.) which thus seems not to be an obstacle for exo-electron emission.

In conclusion, it is believed that monitoring of fatigue using photostimulated electron emission might be feasible. This speculation is based upon the work performed under the present contract, as well as work of other authors.

6.0 ACKNOWLEDGEMENT

This work was supported by the Air Force Office of Scientific Research under Contract No. F44620-71-C-0043.

The authors gratefully acknowledge helpful discussions with Prof. K. L. Kliewer, Ames Laboratory, ERDA, Iowa State University, Ames, Iowa; Dr. R. E. de Wames, Science Center, Rockwell International, Thousand Oaks, California; Prof. T. Wolfram, University of Missouri, Physics Department, Columbia, Missouri; Dr. D. O. Thompson, Science Center, Rockwell International, Thousand Oaks, California. Furthermore, the technical assistance of Mr. J. D. Frandsen, Miss R. J. Richards, Mr. P. J. Stocker, and Mr. R. V. Inman is acknowledged.

7.0 REFERENCES

1. J. Kramer, Der metallische Zustand, Vandenhoeck and Ruprecht, Göttingen, 1950.

2. L. Himmel and P. Kelley, Comments on Solid State Physics, 7, 21 (1976).

3. F. R. Brotzen, Phys. Stat. Solidi, 22, 9 (1967).

4. O. Haxel, F. G. Houtermans, and K. Seeger, Z. Physik, 130, 109 (1951).

5. J. Lohff, Z. Physik, 146, 436 (1956).

6. W. T. Pimbley and E. E. Francis, J. Appl. Phys., 32, 1729 (1961).

7. H. Hassenstein, Naturwiss., 41, 329 (1954).

8. L. Greenberg and K. H. R. Wright, Nature, 174, 657 (1954).

9. A. H. Meleka and W. Barr, Nature, 187, 232 (1960).

10. W. J. Baxter, J. Appl. Physics, 45, 4692 (1974).

11. C. C. Veerman, Mater. Sci. Eng., 4, 329 (1969).

12. V. S. Kortov, R. I. Mints, I. E. Myasnikov and Yu. A. Schevchecko, Phys. Stat. Sol. (a), 2, 55 (1970).

13. R. N. Claytor and F. R. Brotzen, J. Appl. Phys., 36, 3549 (1955).

14. J. E. Moore, S. Tsang, and G. Martin, "The Early Detection of Fatigue Damage," Technical Report AFML-TR-71-185, AF Contract No. F33615-68-C-1706, Sept. 1971.

15. S. A. Hoenig, "Exo-Electron Emission, A New Technique in Non-Destructive Testing," Technical Report AFML-TR-71-140, Dec. 1971.

16. P. Braunlich, J. Carrico, R. Rosenblum, and L. Himmel, "The Mechanism of Exo-Electron Emission," Bendix Corporation Report, Sept. 1973.

17. L. Himmel in Proceedings of the Interdisciplinary Workshop for Quantitative Flaw Detection, Technical Report AFML-TR-74-238, Nov. 1974, p. 503.

18. W. J. Baxter, J. Appl. Phys., 44, 4400 (1973).

19. D. O. Thompson, R. A. Young, G. A. Alers, and T. Smith, J. Appl. Phys., 47, 3846 (1976).

20. O. Buck, W. J. Pardee, F. J. Szalkowski, and D. O. Thompson, Appl. Phys., in press.

21. W. J. Baxter and S. R. Rouze, Met. Trans., 7A, 647 (1976).

22. J. G. Endriz and W. E. Spicer, Phys. Rev., B4, 4159 (1971).

23. A. Nourtier, Annales de Physique (Paris) 8, 443 (1973).

24. A. A. Maradudin and D. L. Mills, Phys. Rev., B11, 1392 (1975).

25. V. Celli, A. Marvin and F. Toigo, Phys. Rev., B11, 1779 (1975).

26. A. Marvin, F. Toigo, and V. Celli, Phys. Rev., B11, 2777 (1975).

27. W. J. Baxter, Metallurgical Transactions, 6A, 749 (1975).

28. O. Buck, W. J. Pardee, F. J. Szalkowski, and J. M. Curnow, Rockwell International Science Center Report No. SC573.4IR, Contract No. F44620-74-C-0043 (1976).

29. W. J. Pardee and O. Buck, Materials Evaluation-Research Supplement (accepted for publication).

30. W. J. Pardee and O. Buck, to be submitted to Appl. Physics.

31. W. F. Krolikowski, "Photoemission Studies of the Noble Metals, the Cuprous Halides and Selected Alkali Halides," Technical Report No. 5218-1, Stanford Electronics Laboratories, Stanford, CA, May 1967.

32. J. C. Grosskreutz, Phy. Stat. Sol. (b) 47, 11 (1971).

33. J. C. Grosskreutz, Phy. Stat. Sol. (b) 47, 359 (1971).

34. O. Buck, IEEE Transactions on Sonics and Ultrasonics, SU-23, 283 (1976).

35. W. L. Morris, O. Buck, and H. L. Marcus, Met. Trans. 7A, 1161 (1976).

36. W. J. Baxter and S. R. Rouze, Met. Trans. 7A, 647 (1976).

37. J. F. Moore, S. Tsang, D. O. Thompson, and S. A. Hoenig, "Nondestructive Detection of Structural Damage Uniquely Associated with Fatigue," Technical Report AFML-TR-74-131, July 1974.

8.0 BIBLIOGRAPHY

The work discussed in the present report was performed between January 1, 1974, and December 31, 1976. Several reports, in addition to the present Final Report, and publications have resulted from this work as outlined below.

8.1 Previous Reports Resulting from Contract No. F44620-71-C-0043

(1) O. Buck, "Mechanisms of Exo-Electron Emission in Structural Materials," Rockwell International Science Center Report No. SC573.2IR, Progress Report for the Period January 1, 1974, to February 15, 1975.

(2) O. Buck, W. J. Pardee, F. J. Szalkowski, and J. M. Curnow, "Mechanisms of Exo-Electron Emission in Structural Materials," Rockwell International Science Center Report No. SC753-4IR, Progress Report for the Period February 16, 1975, to December 31, 1975.

8.2 Publications Resulting from Contract No. F44620-71-C-0043

(1) F. J. Szalkowski, "Energy Distribution of Photo-Stimulated Electron Emission from Fatigue Specimens," in Proceedings of the Interdisciplinary Workshop for Quantitative Flaw Detection, Technical Report AFML-TR-74-238, Nov. 1974, p. 507.

(2) O. Buck, "Energy Dependence of Fatigue-Enhanced Photoemission," in Proceedings of the ARPA/AFML Review of Quantitative NDE. Technical Report AFML-TR-75-212, January 1976, p. 681.

(3) O. Buck, W. J. Pardee, F. J. Szalkowski, and D. O. Thompson, "Deformation Enhanced Photoemission from Aluminum. I. Experimental Results," Applied Physics (in press).

(4) W. J. Pardee and O. Buck, "U.V. Photoemission as a Measure of Plastic Deformation," Materials Evaluation - Research Supplement (accepted).

(5) W. J. Pardee and O. Buck, "Deformation Enhanced Photoemission from Aluminum. II. Theory," to be submitted to Applied Physics.

(6) O. Buck, W. J. Pardee, and J. M. Curnow, "Fatigue Enhanced Photoemission (Exo-electrons)" to be submitted to Metallurgical Transactions.

(7) O. Buck and W. J. Pardee, "Advances and Qualification of Exo-Electron Spectroscopy," to be submitted to Symposium on Electron and Positron Spectroscopies in Materials Science and Engineering. Academic Press, Fall, 1977.

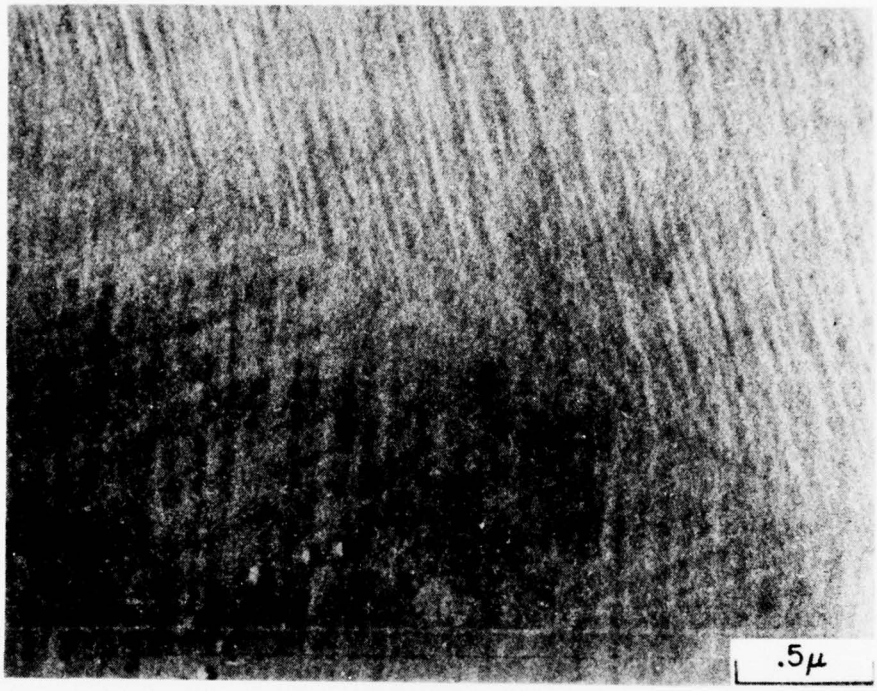


Fig. 1 Surface replica of Al 1100 (HO) after 4000 cycles, showing a dense slipline pattern.

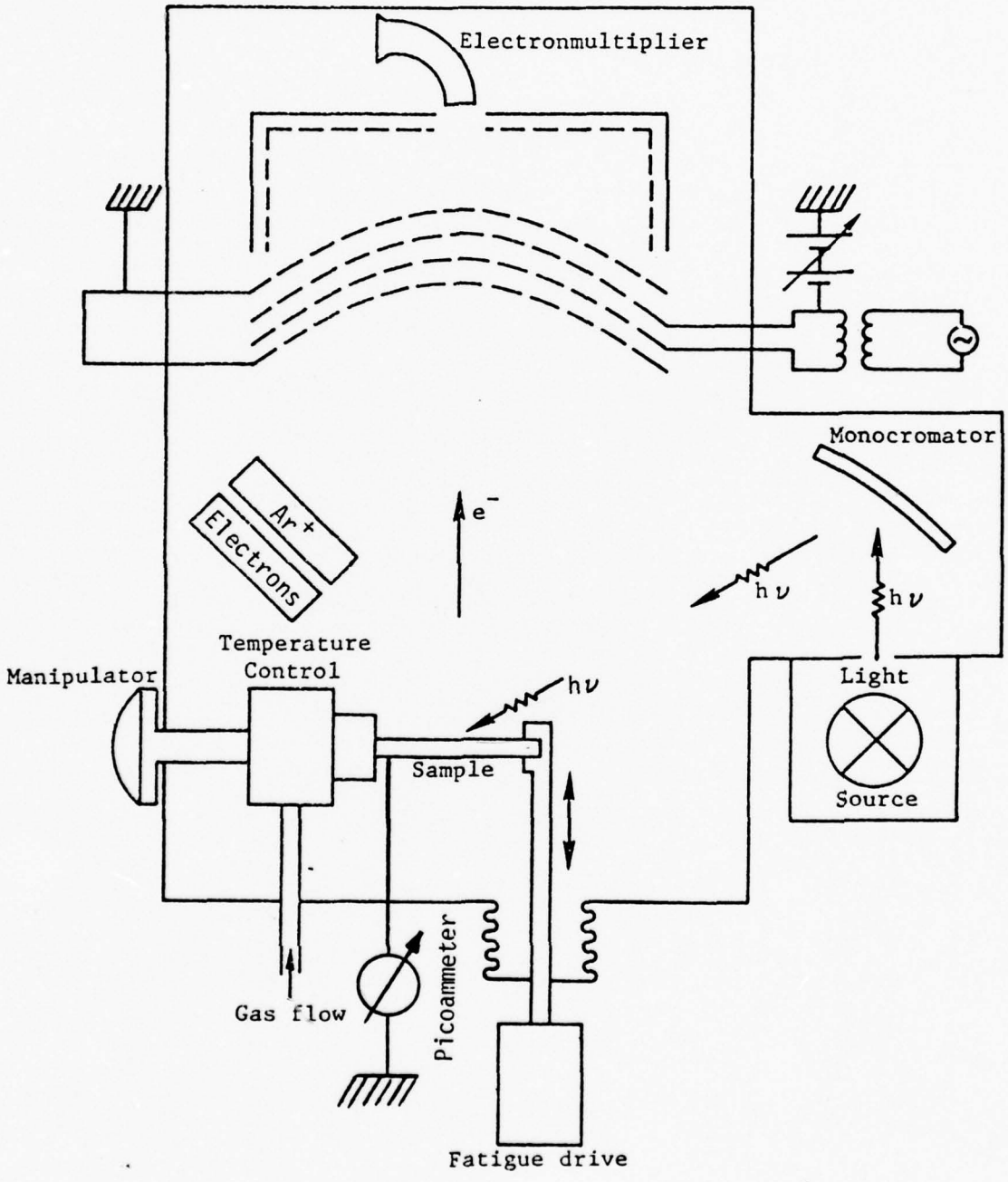


Fig. 2 Schematic diagram of ultra-high vacuum system to determine fatigue enhanced photoemission.

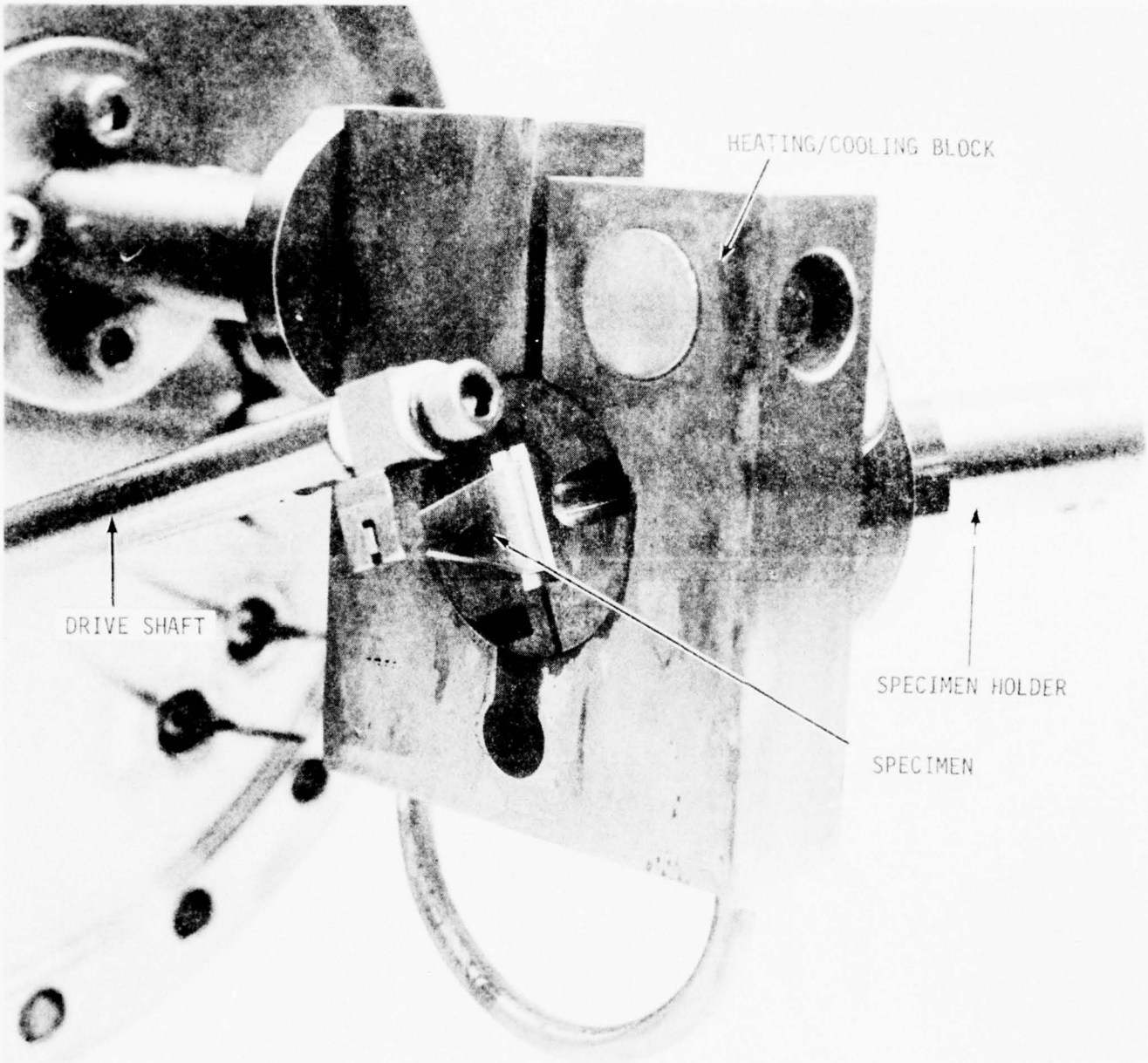


Fig. 28 Photoyield of etched titanium as a function of incident energy and fatigue.

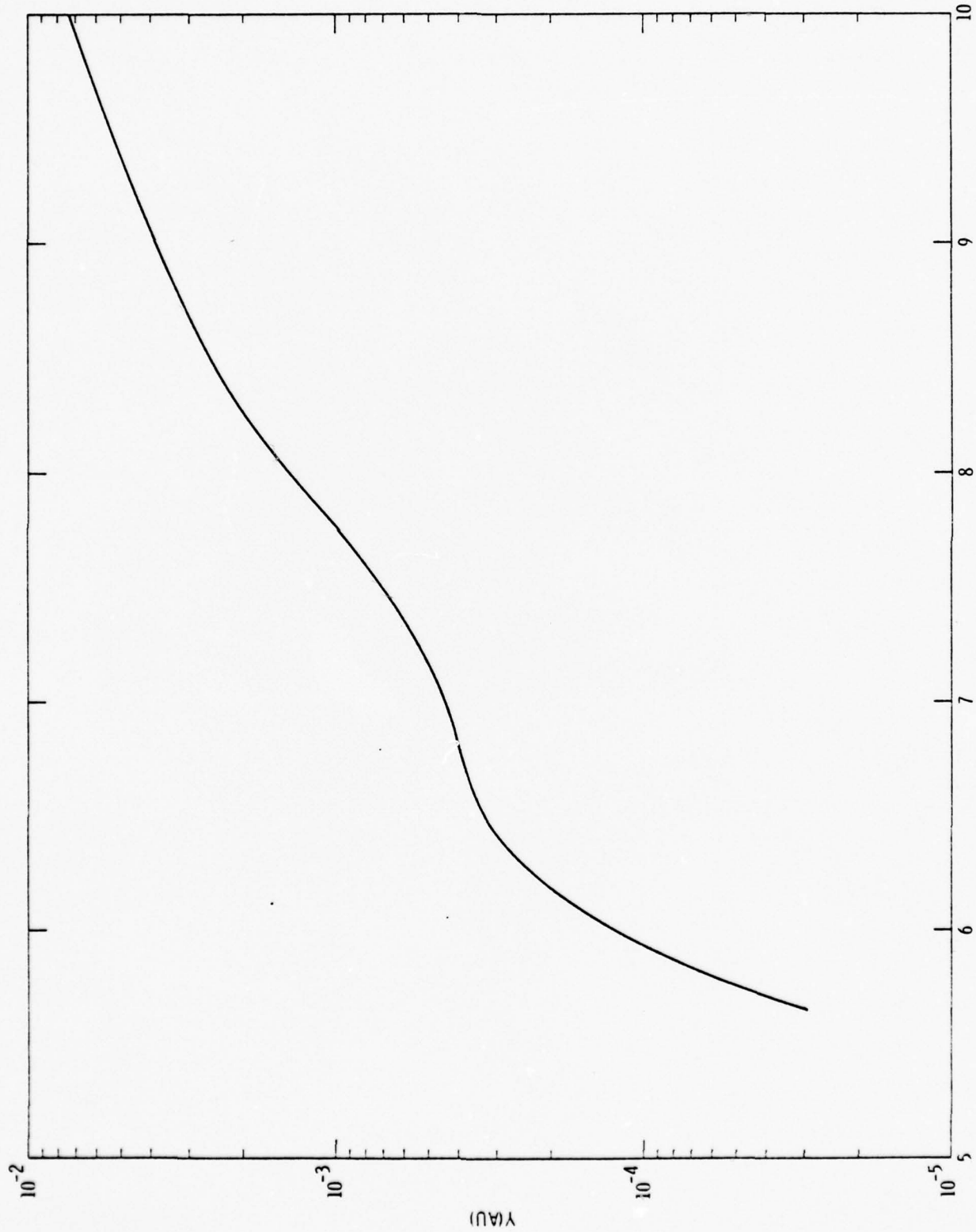


Fig. 4 Photoyield of gold as a function of incident photon energy.

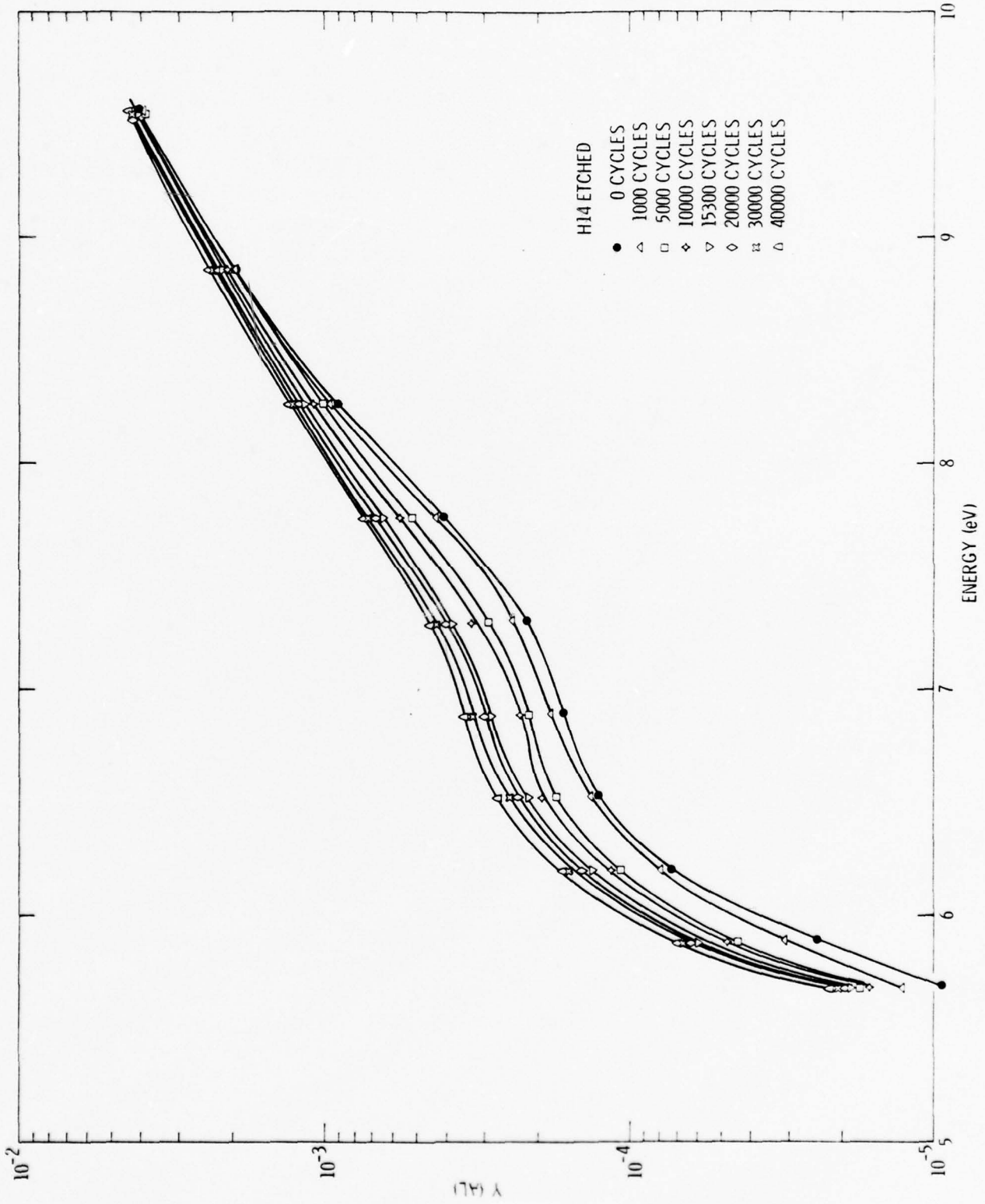


Fig. 5 Photoyield of etched Al 1100 (H14) as a function of incident energy and fatigue.

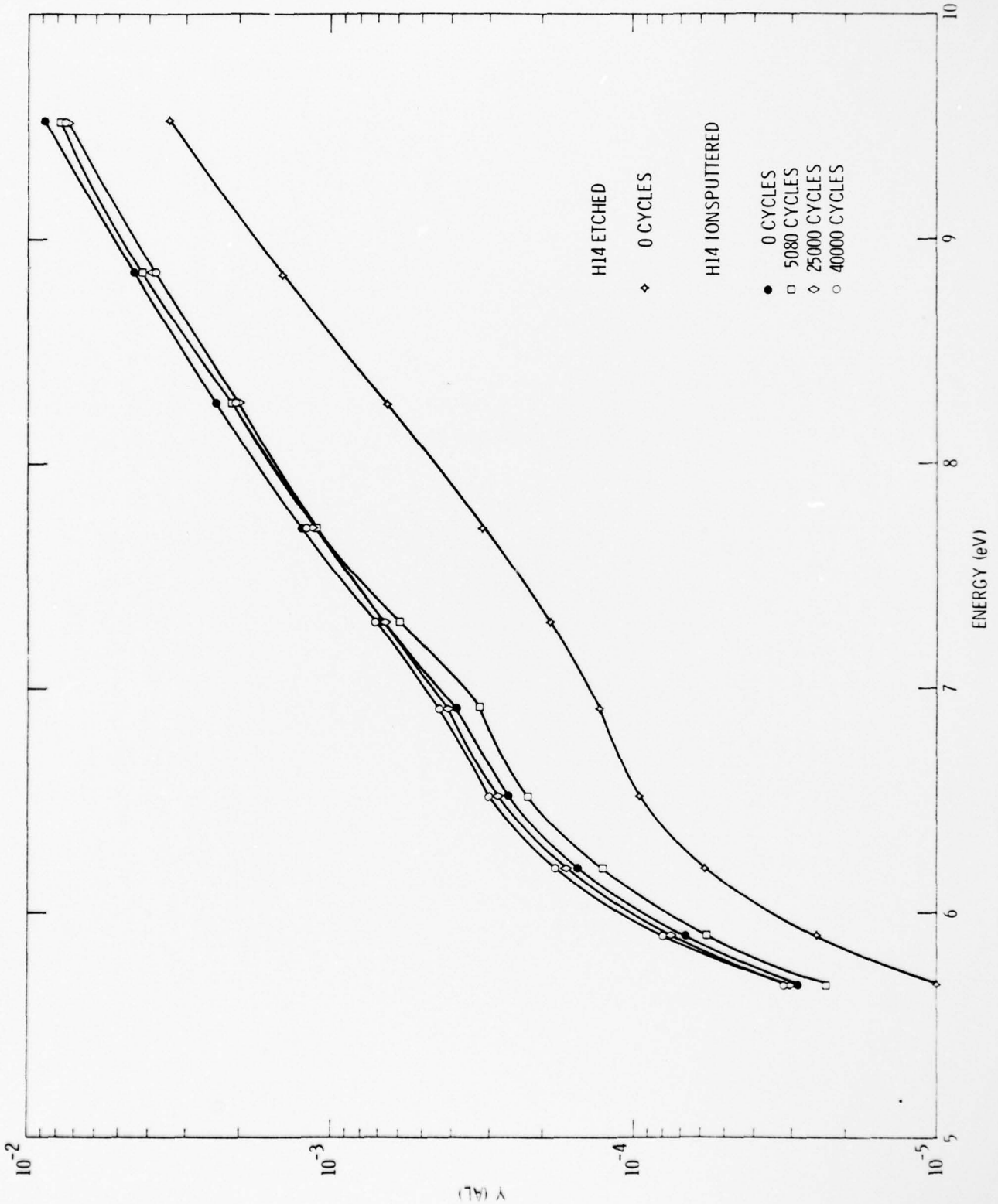


Fig. 6 Photoyield of etched and ion sputtered Al 1100 (H14) as a function of incident energy and fatigue.

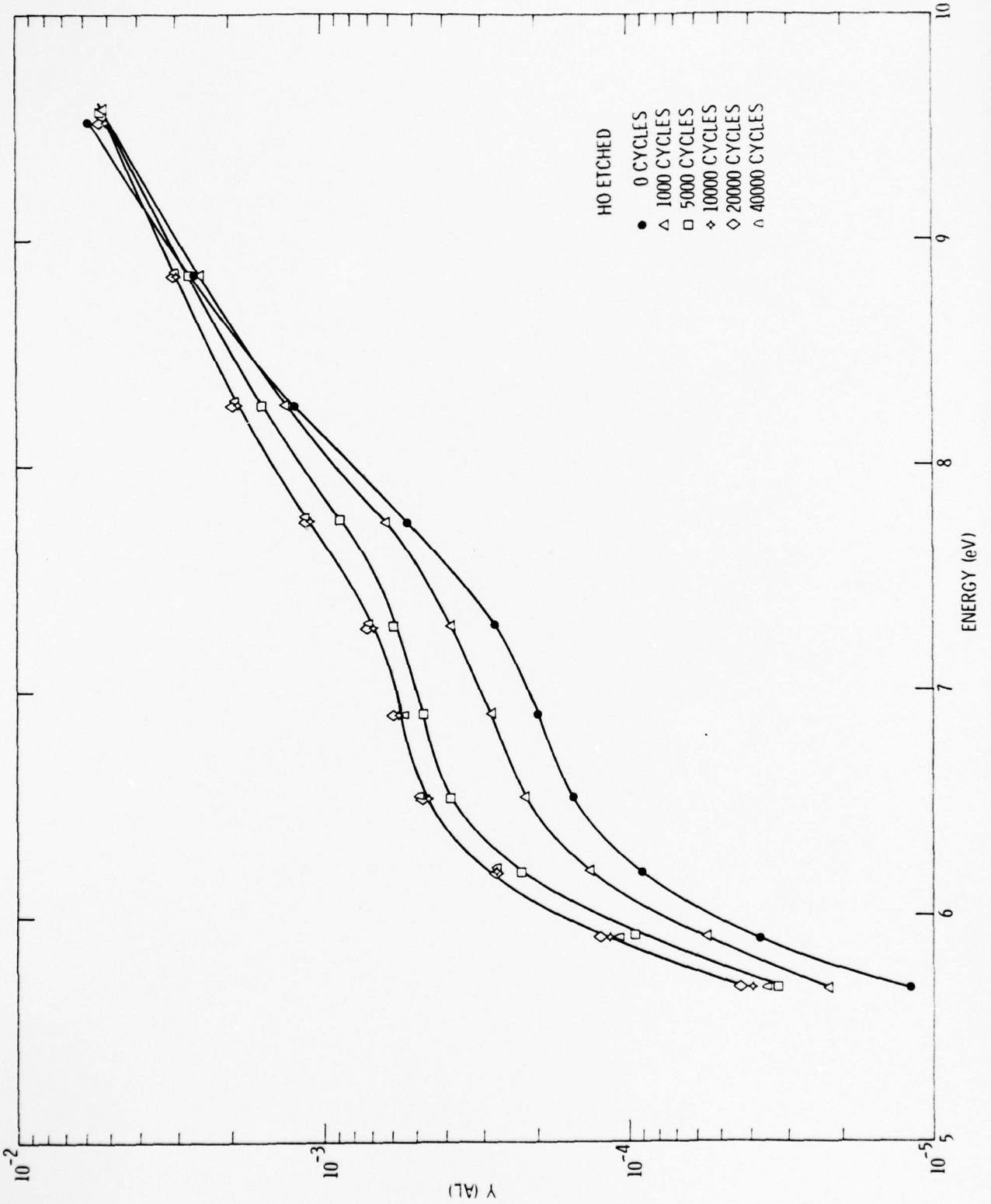


Fig. 7 Photoyield of etched Al 1100 (HO) as a function of incident energy and fatigue.

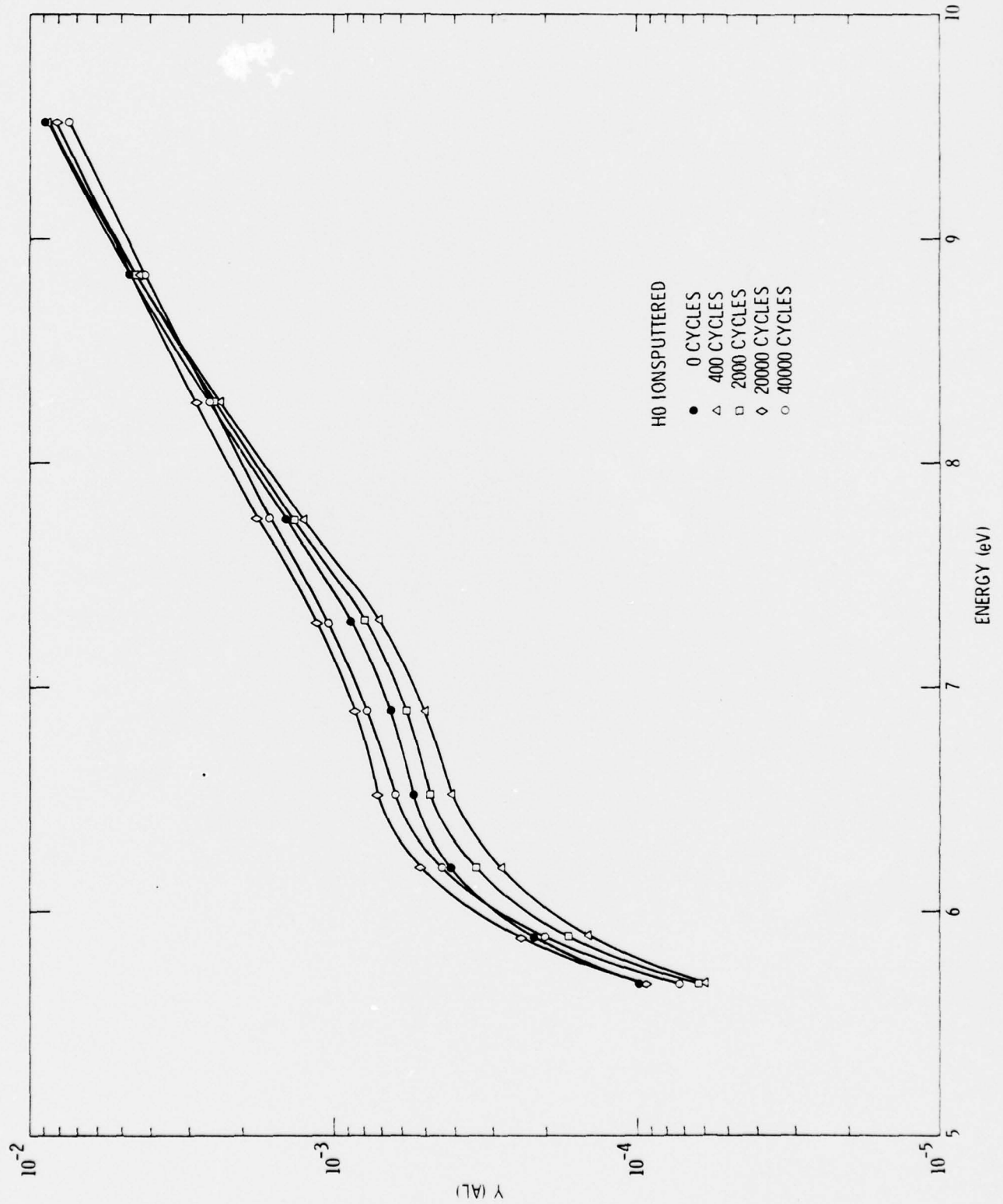


Fig. 8 Photoyield of ion sputtered Al 1100 (HO) as a function of incident energy and fatigue.

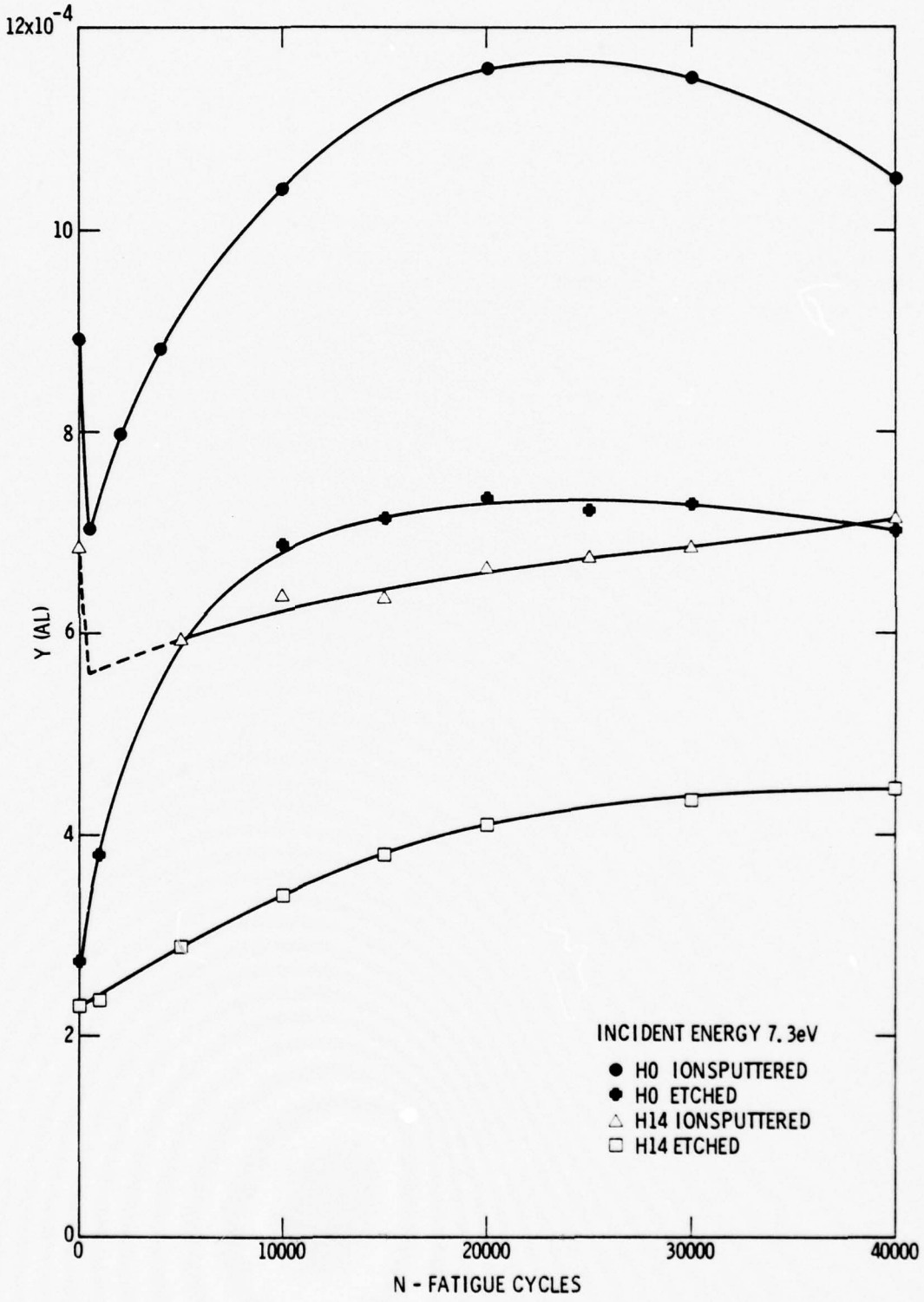


Fig. 9 Photoyield of Al 1100 (H0 and H14) as a function of fatigue (at 7.3 eV).

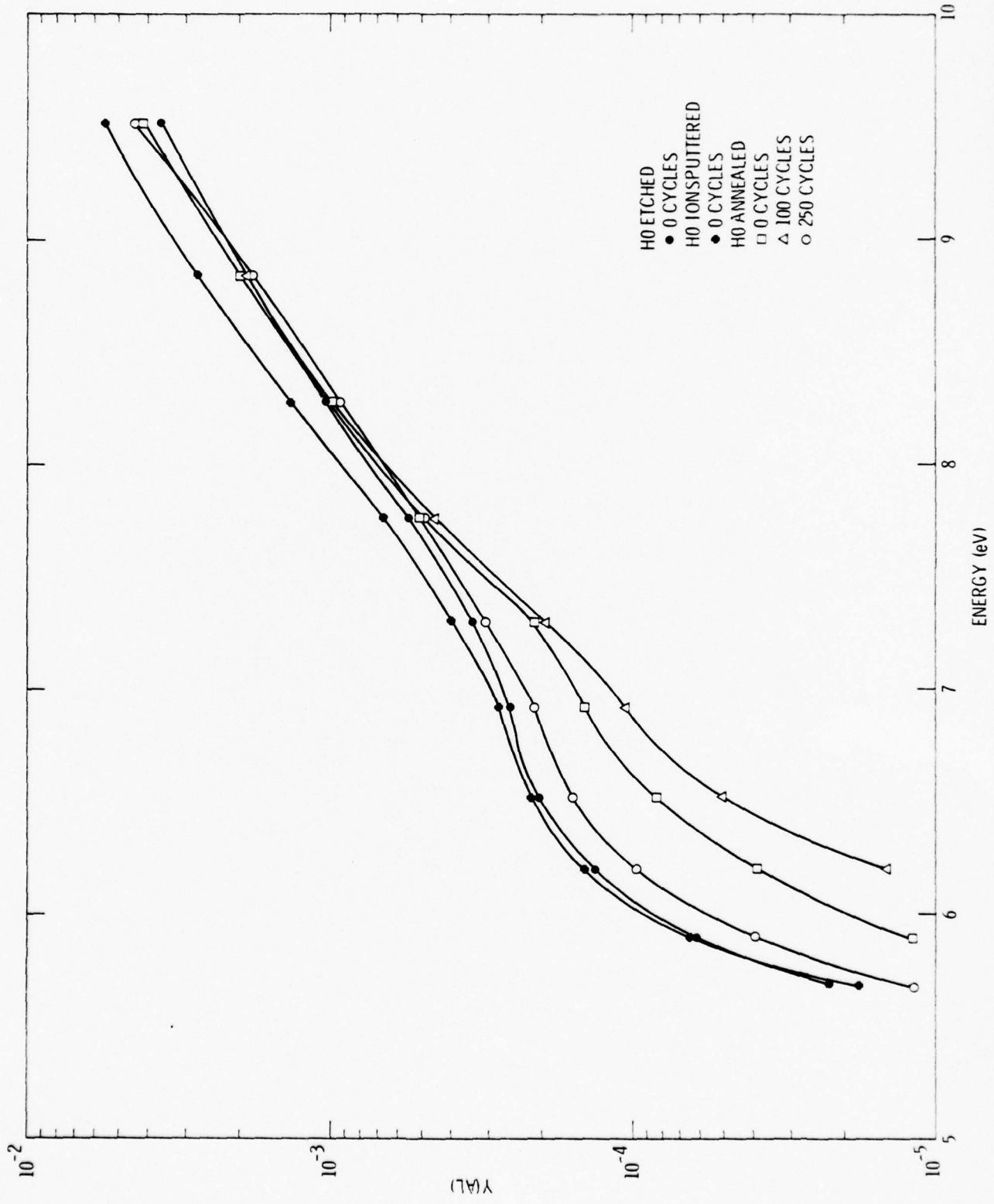


Fig. 10 Photoyield of etched, ion-sputtered and quenched Al 1100 (HO) as a function of incident energy and fatigue.

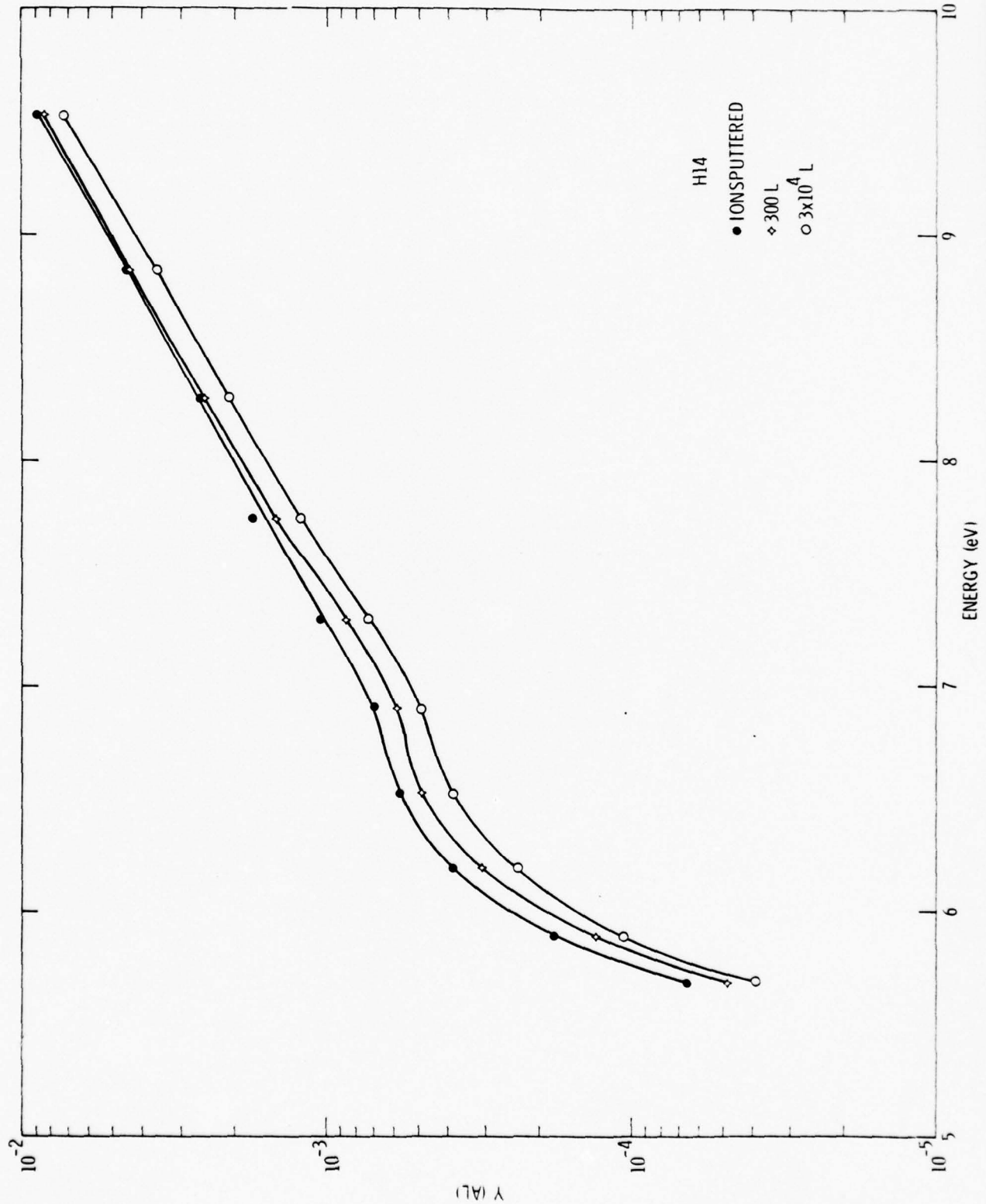


Fig. 11 Photoyield of ion sputtered Al 1100 (H14) as a function of oxide redeposition.

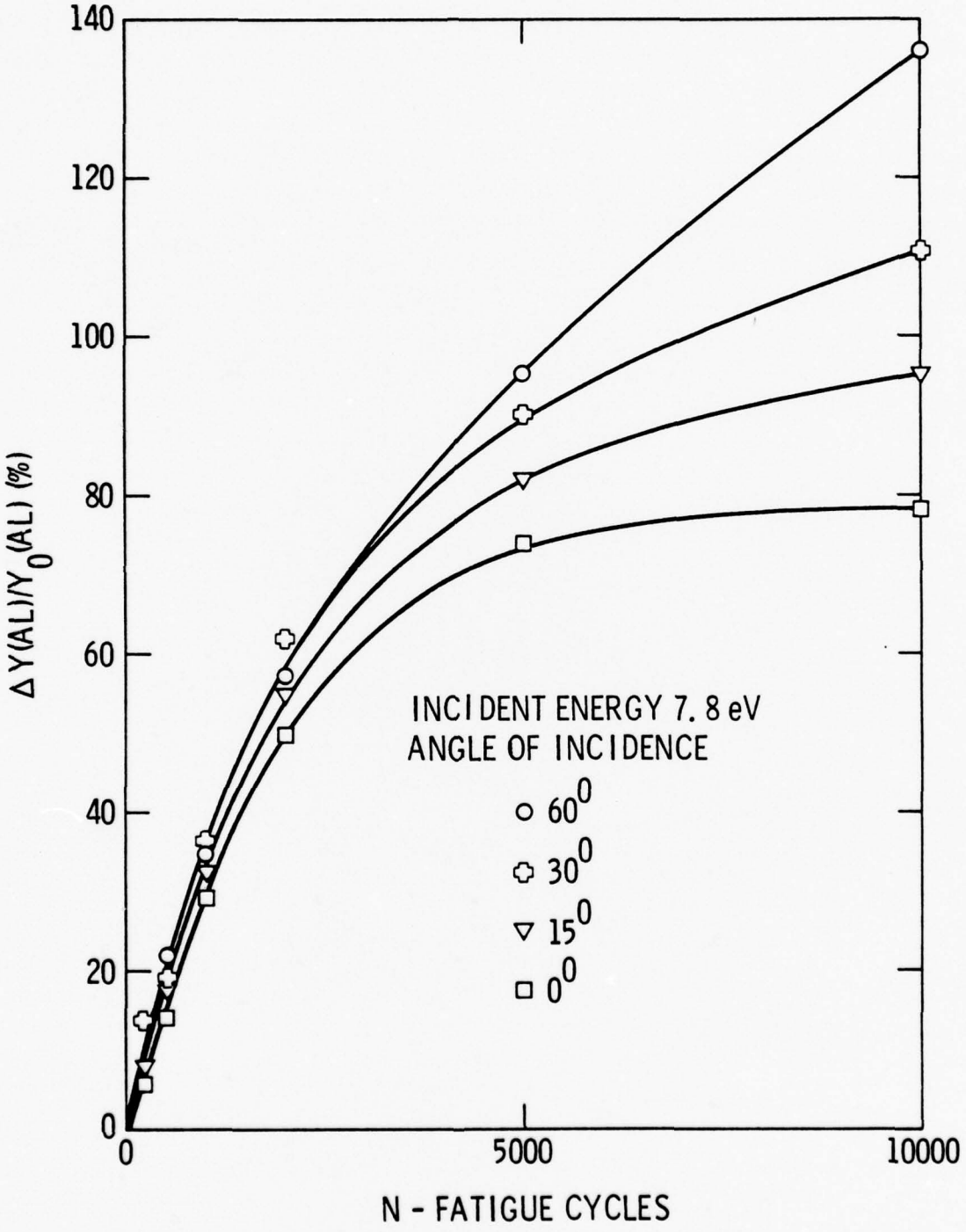
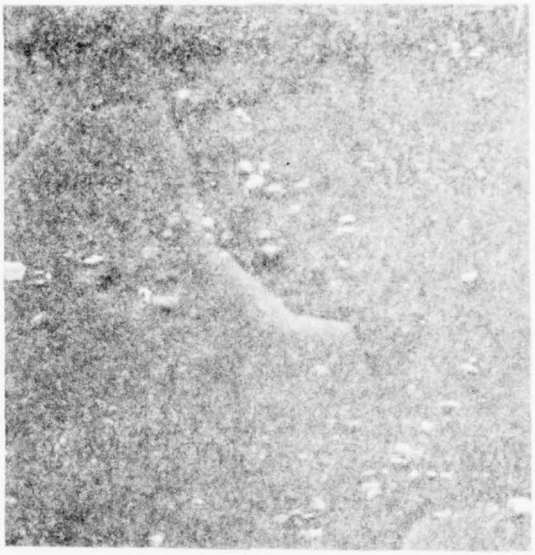
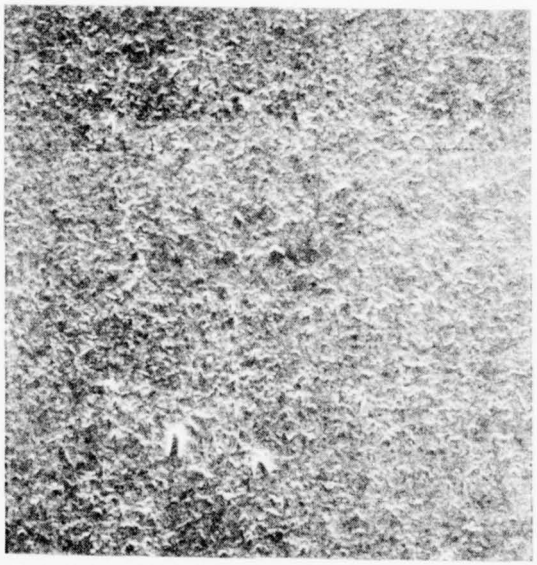


Fig. 12 The relative change of the photoyield as a function of fatigue and cycle of incidence of photons (at 7.8 eV).

Rockwell International
Science Center



(a) ETCHED



10 µm

(b) 10 µm GRIT



(c) 50 µm GRIT

Fig. 13 Comparison of surface roughness due to shot-peening with Al_2O_3 particles prior to fatigue (SEM).

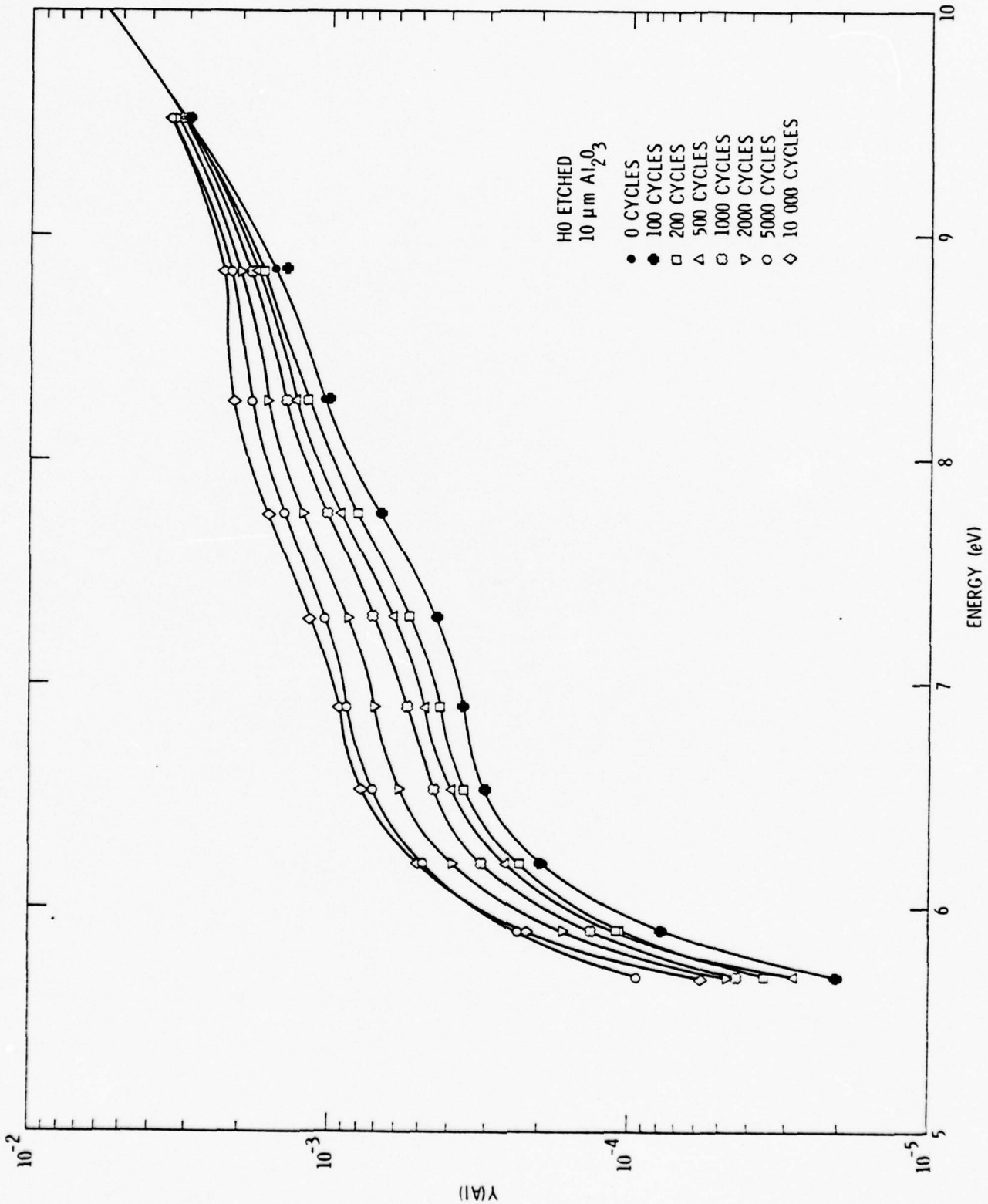


Fig. 14 Photoyield of shot-peened (10μm Al_2O_3 particles) and etched Al 1100 (H0) as a function of incident energy and fatigue.

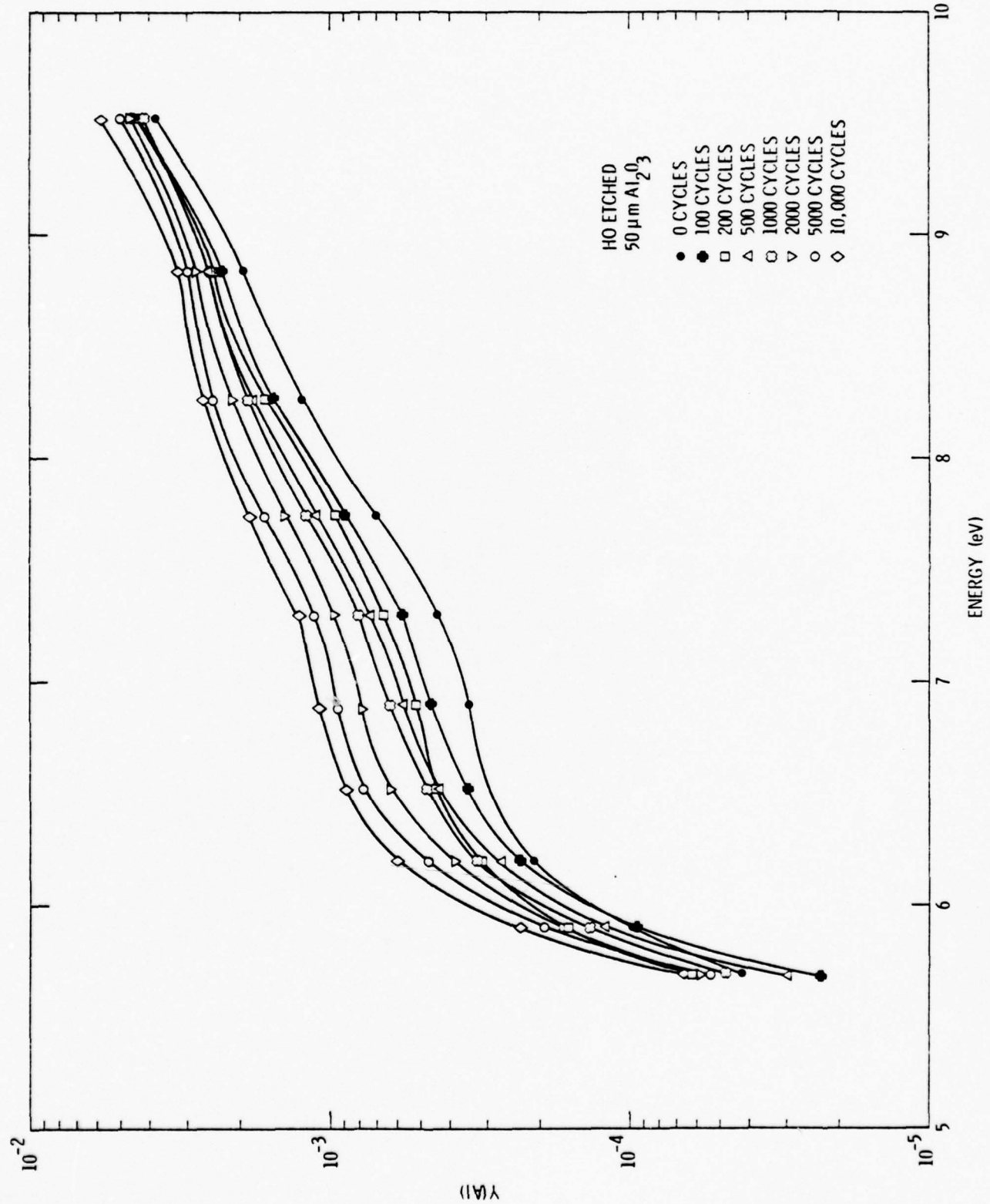


Fig. 15 Photoyield of shot-peened and etched (50μm Al_2O_3 particles) Al 1100 (HO) as a function of incident energy and fatigue.

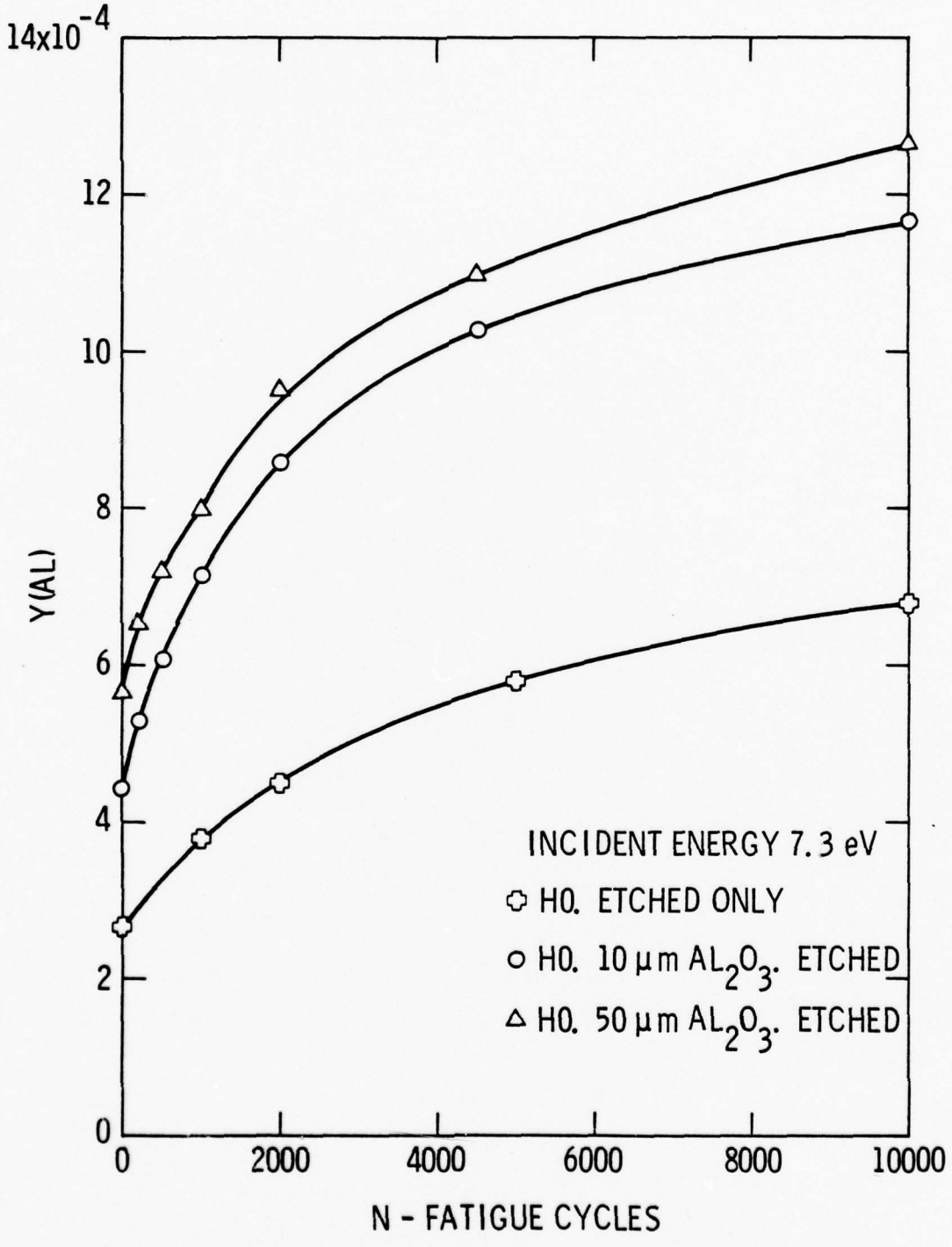


Fig. 16 Photoyield of Al 1100 (HO) after different degrees of shot-peening as a function of fatigue (at 7.3 eV).

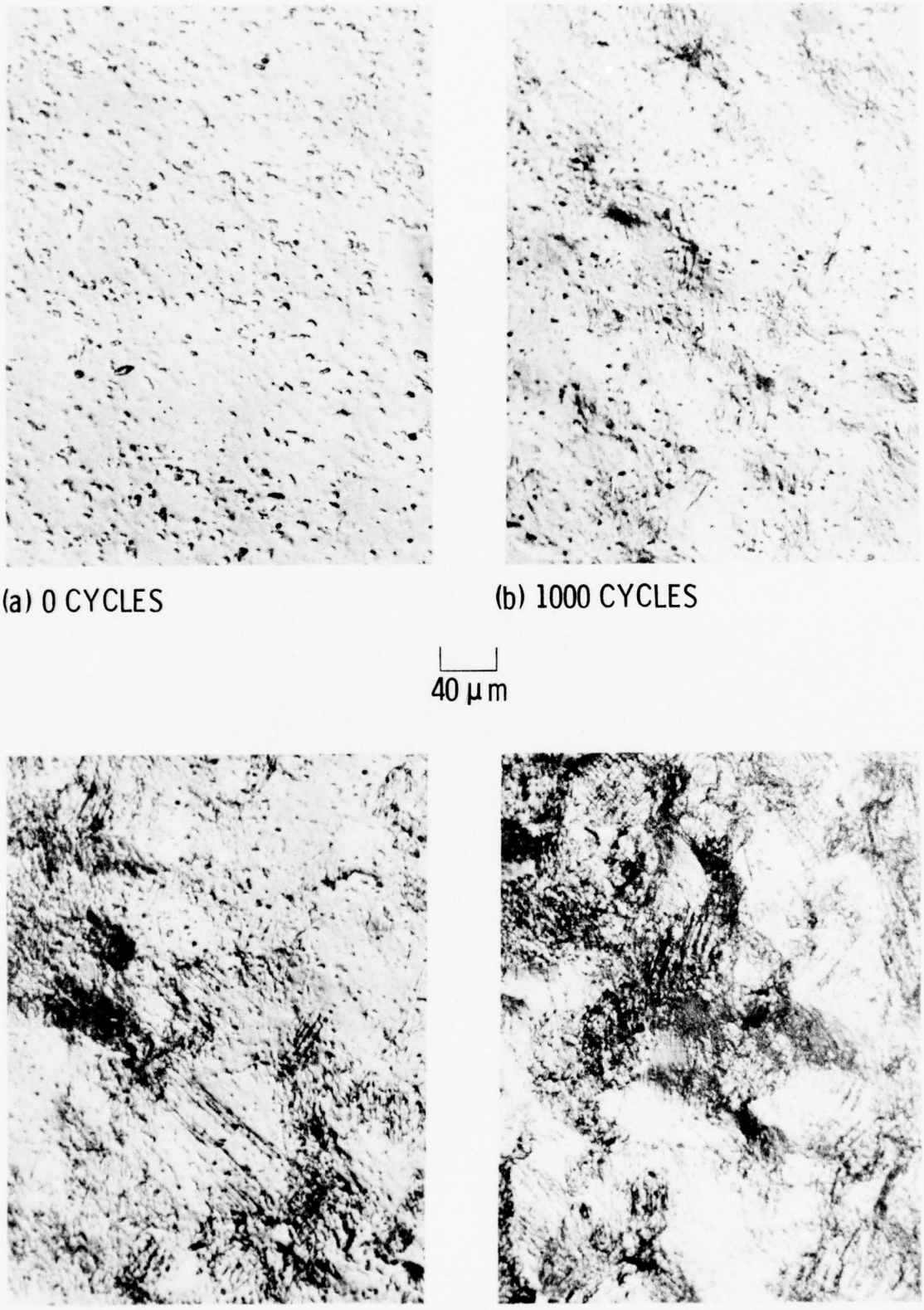


Fig. 17 Development of surface slip on Al 1100 (HO) as a function of fatigue (optical micrographs of etched surfaces).

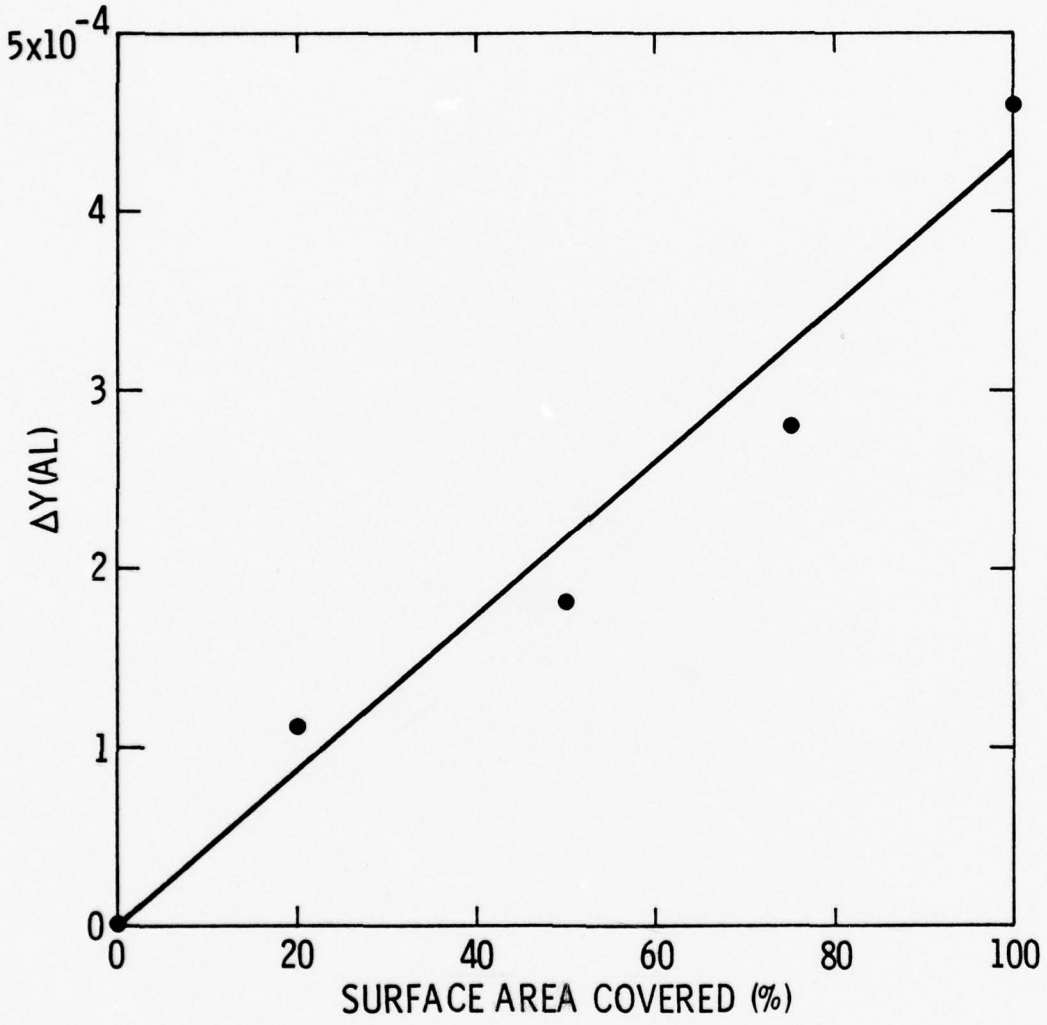
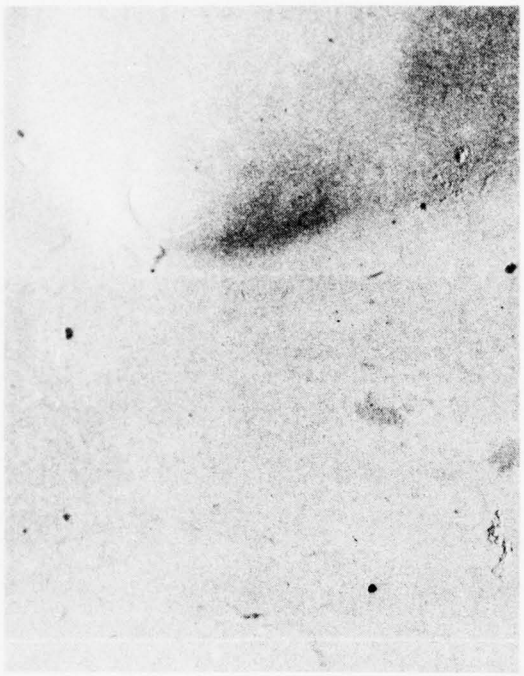


Fig. 18 The change of photoyield (at 7.3 eV) with surface area covered by slip. Material: Al 1100 HO.



(a) 0 CYCLES



(b) 1000 CYCLES

2 μm



(c) 2000 CYCLES



(d) 4000 CYCLES

Fig. 19 Slip line traces at different states of fatigue (surface replicas).

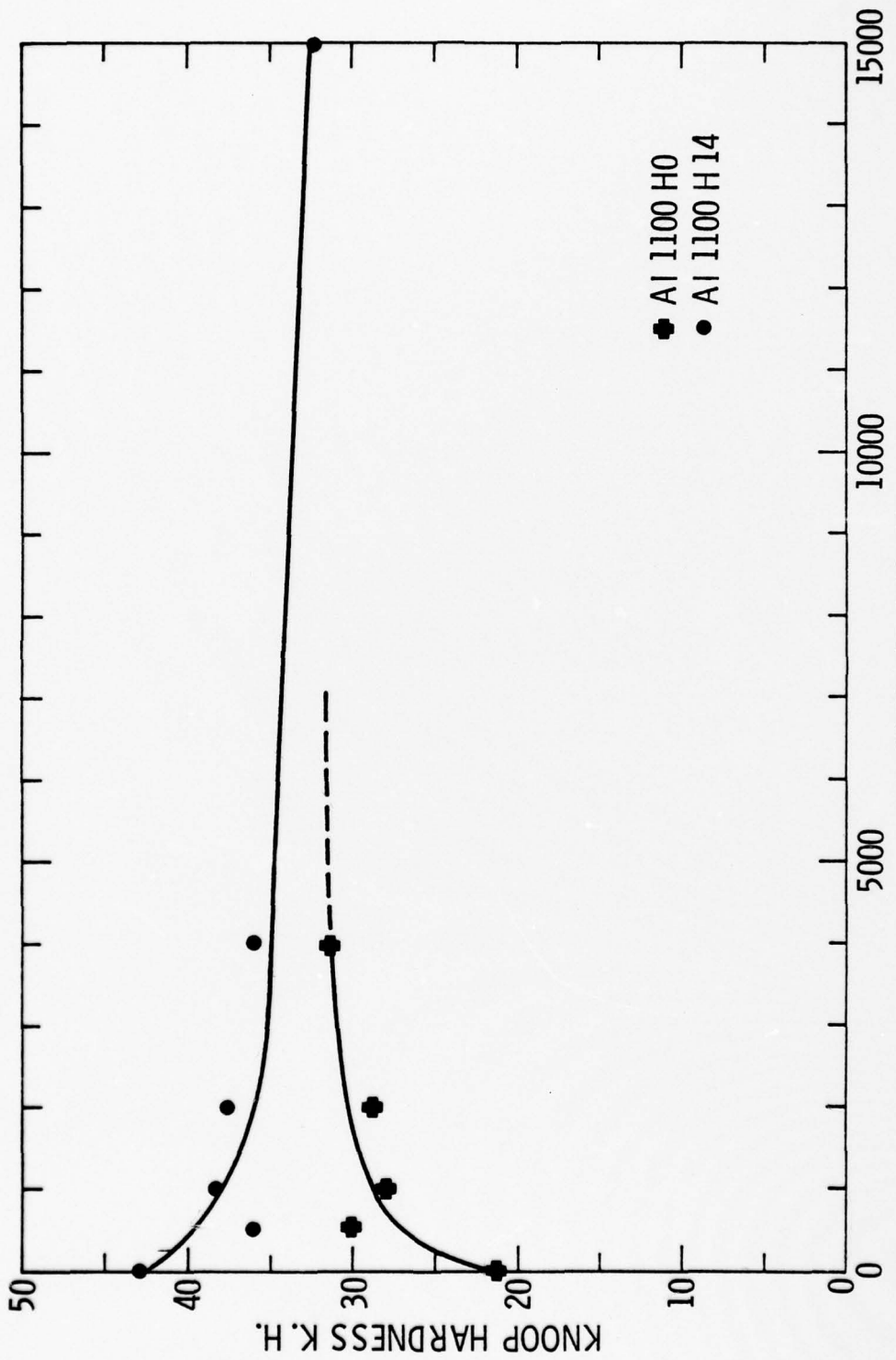


Fig. 20 Comparison of the Knoop hardness, K.H., for Al 1100 HO and Al 1100 H14 as a function of fatigue.



Fig. 21 X-ray Laue pattern and slip line development on Al single crystal.

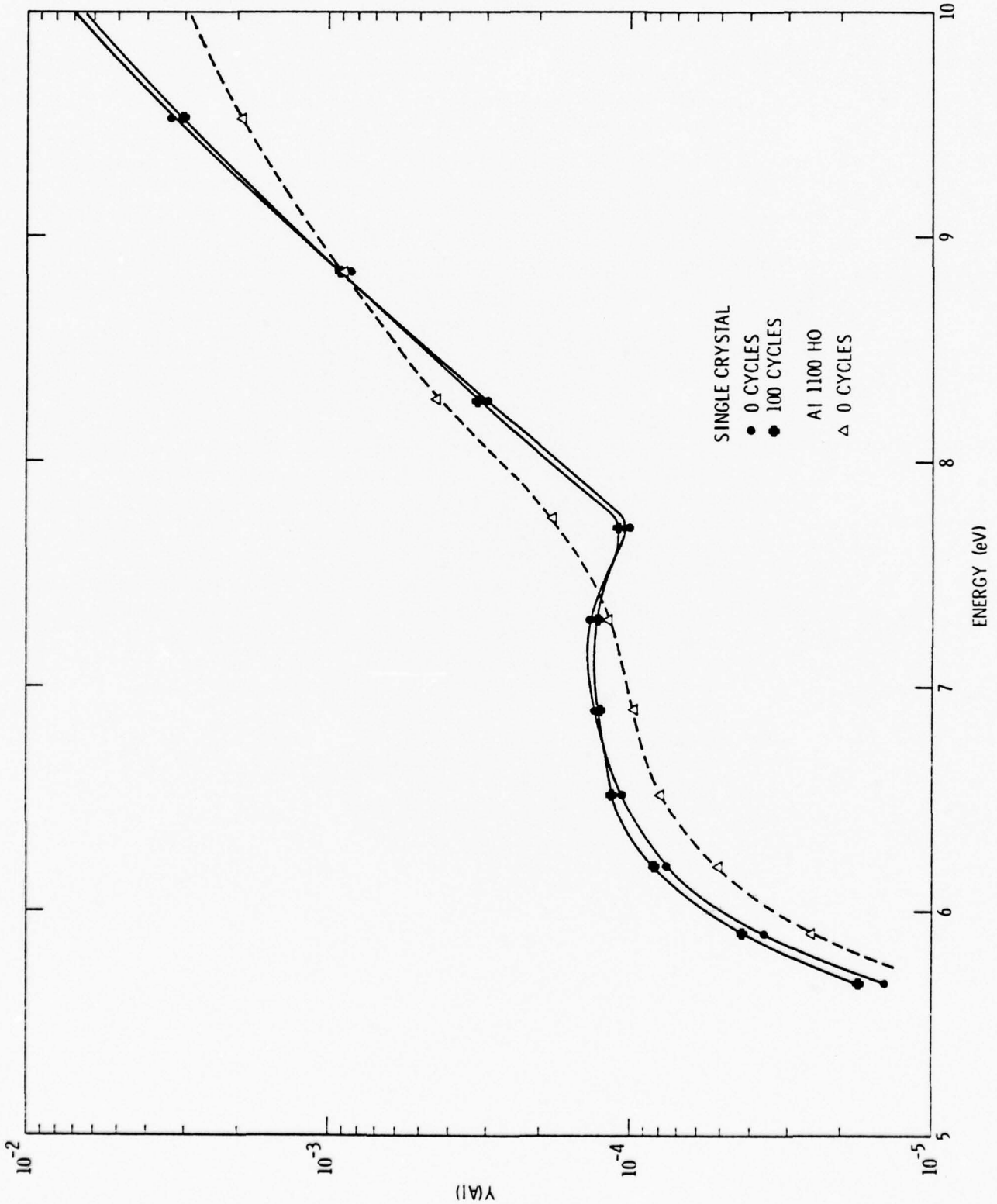


Fig. 22 Photoyield of Al single crystal compared with Al 1100 HO

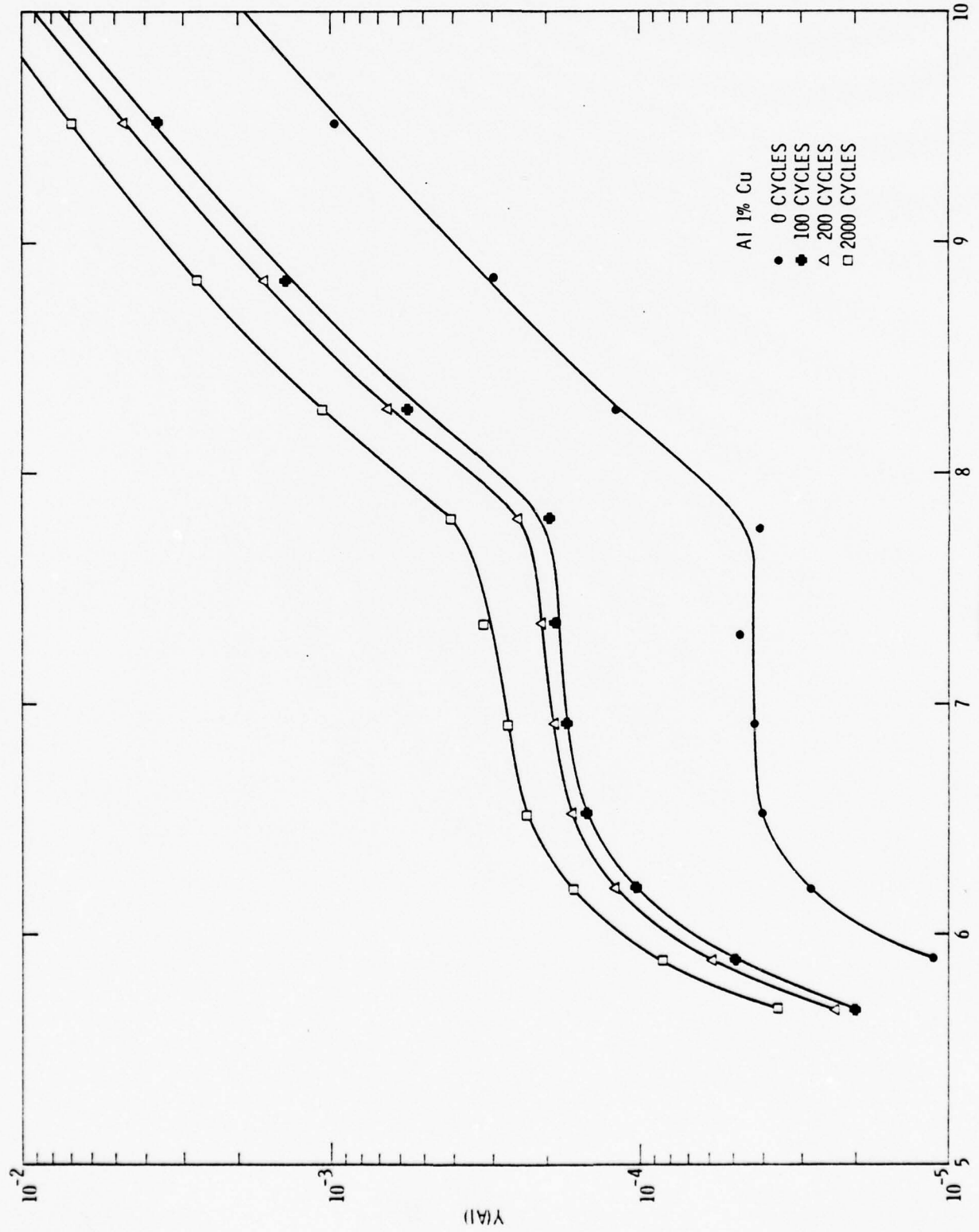


Fig. 23 Photoyield of etched Al 1%Cu as a function of incident energy and fatigue.

SC573.5FR

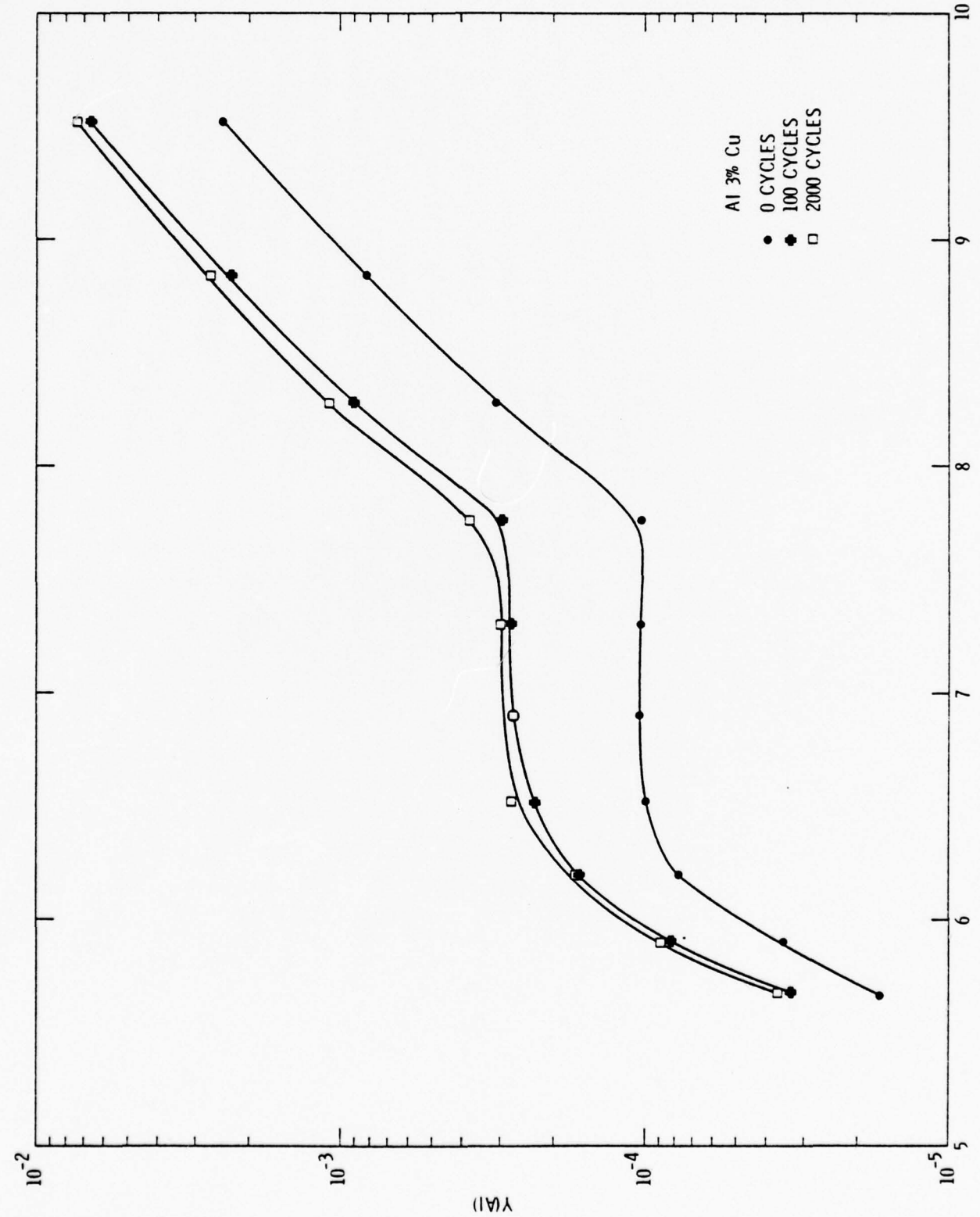


Fig. 24 Photoyield of etched Al 3%Cu as a function of incident energy and fatigue.

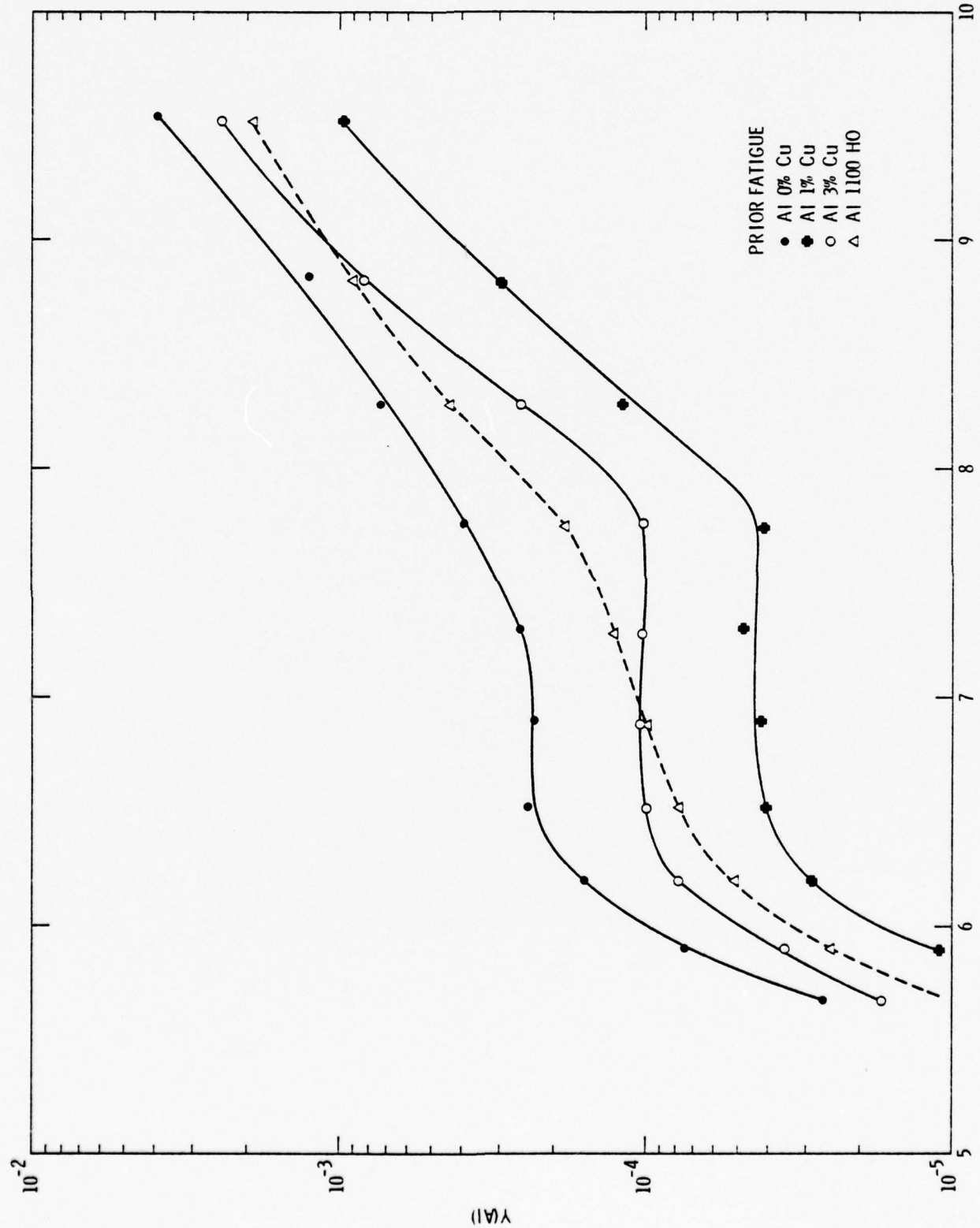


Fig. 25 Photoyield of Al 0%Cu, Al 1%Cu and Al 3%Cu compared with Al 1100 HO (prior to fatigue).

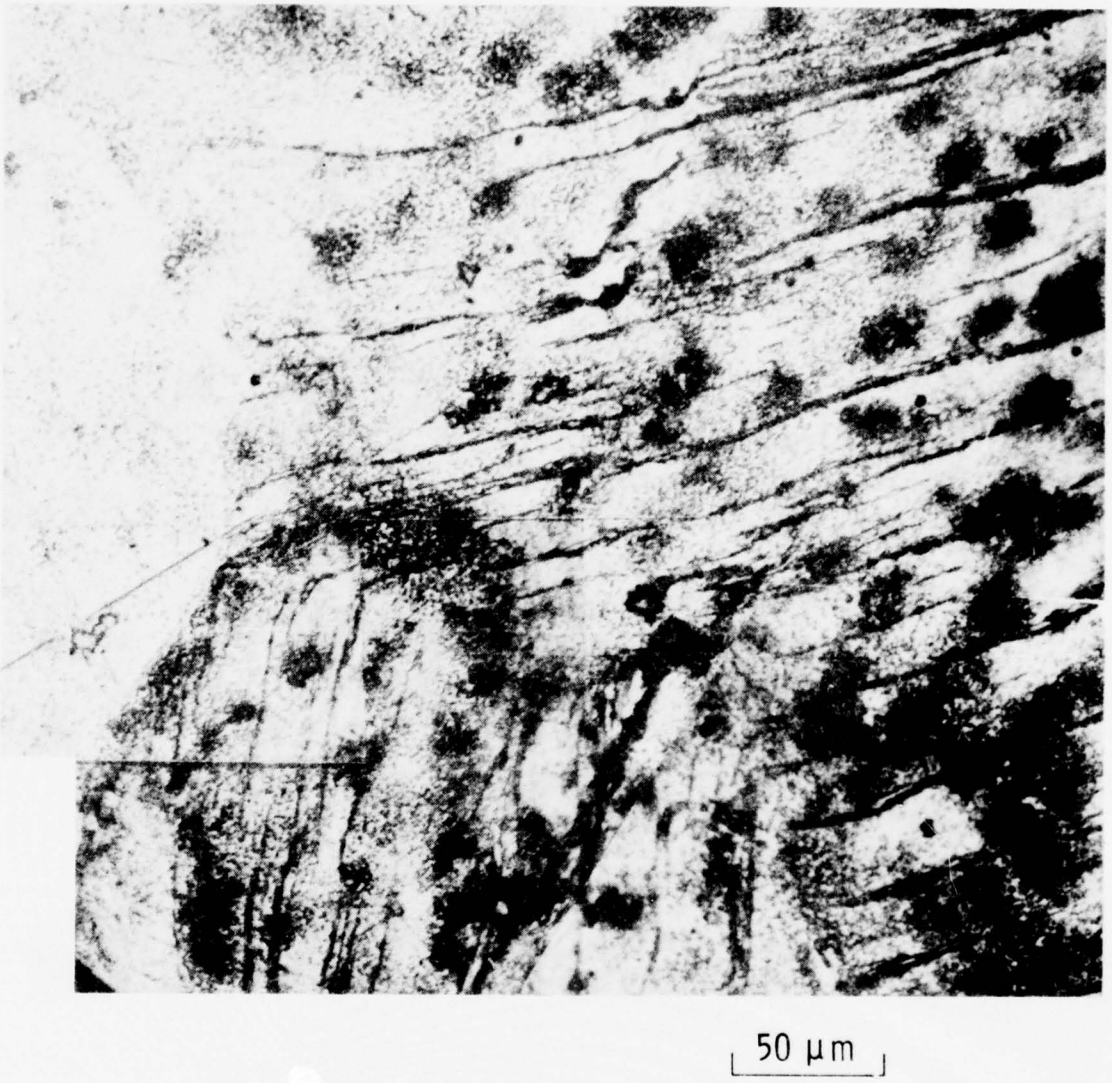


Fig. 26 Slip line traces developed after 4000 cycles of fatigue (failure) of Al 1%Cu.

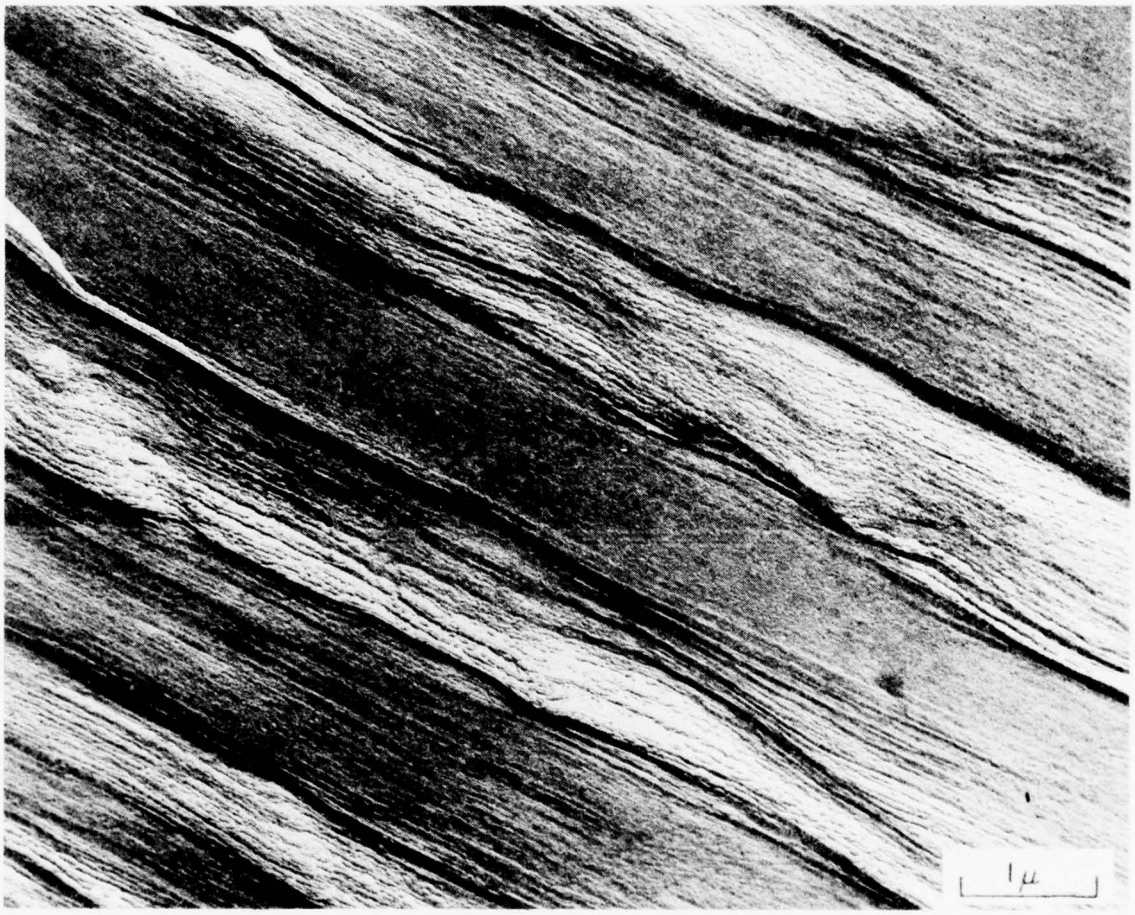


Fig. 27 Surface replica of Al 1%Cu fatigued for 250 cycles.

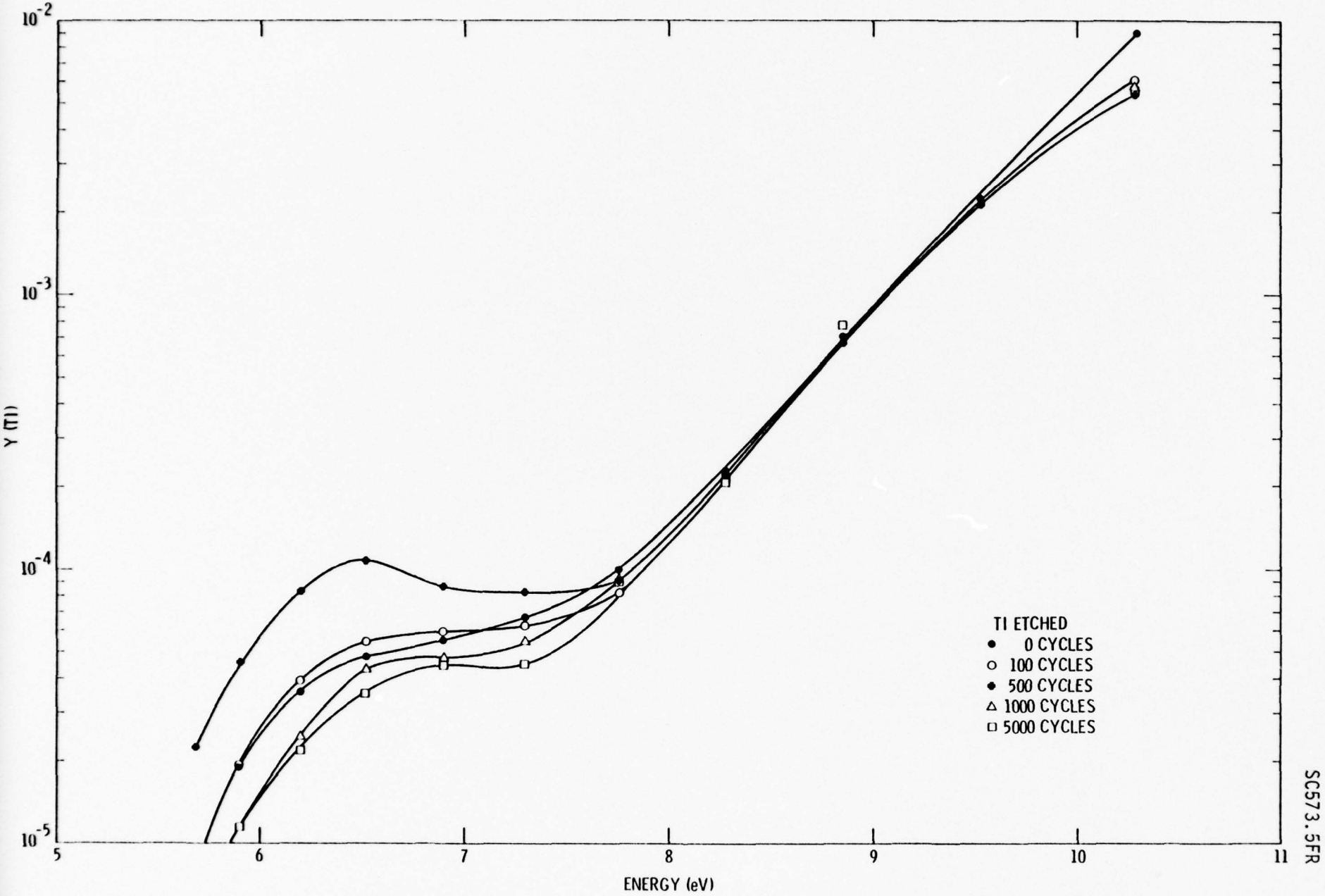


Fig. 28 Photoyield of etched titanium as a function of incident energy and fatigue.

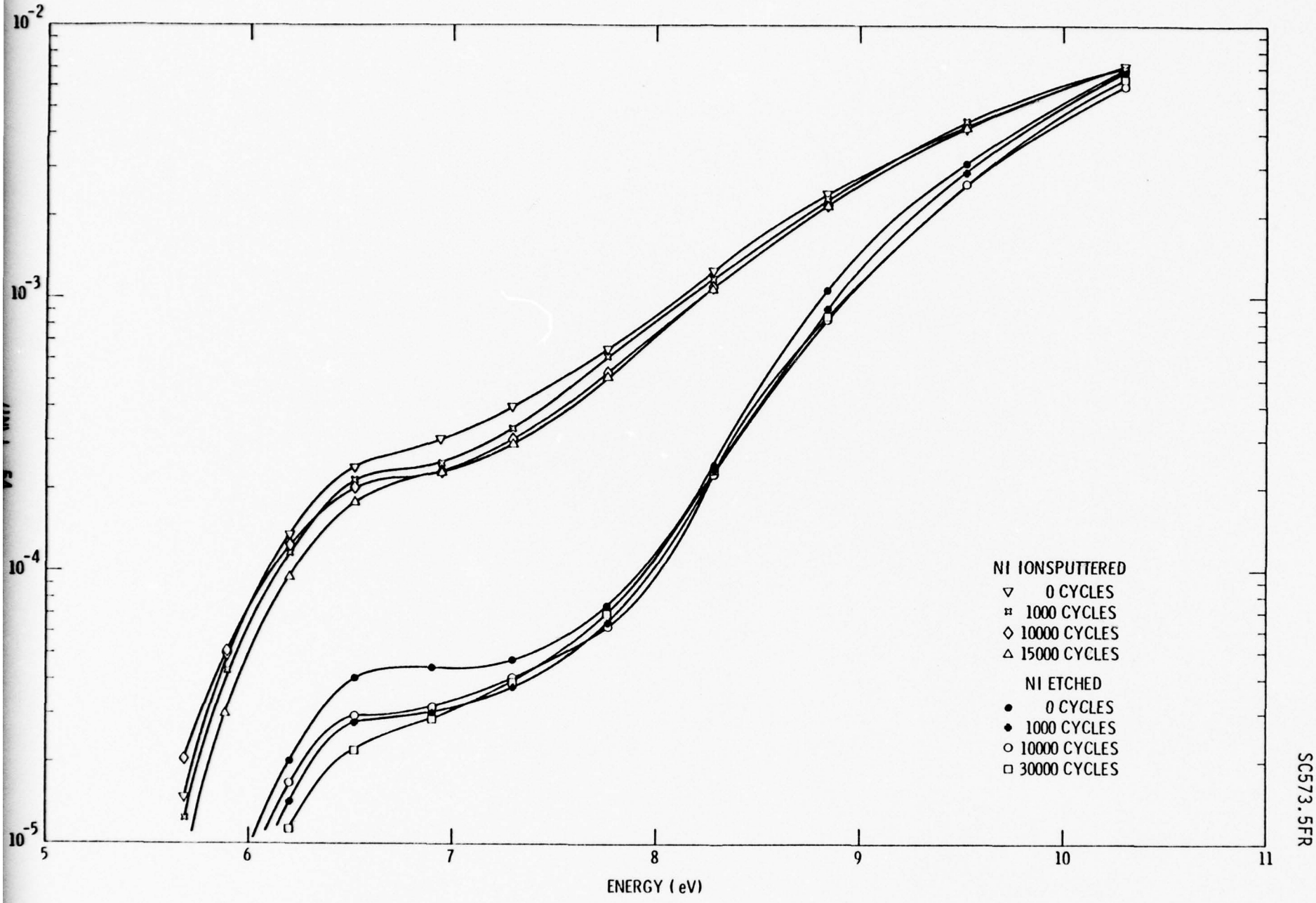


Fig. 29 Photoyield of ion sputtered and etched nickel as a function of incident energy and fatigue.

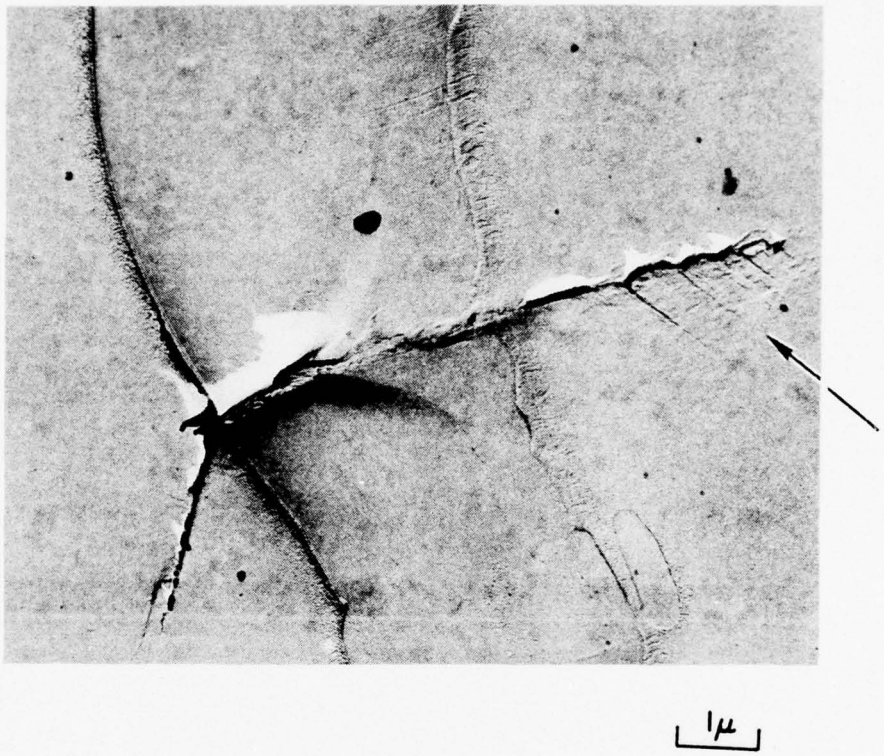


Fig. 30 Surface replica of Al 2219 T851, showing a crack initiated at an intermetallic. Slip line development indicated by arrow.

APPENDIX

THE THEORETICAL BASIS FOR EXO-ELECTRON EMISSION (ROUGHNESS INDUCED PHOTOEMISSION)

During the extensive experimental measurements, summarized in the present report, it became clear that a full understanding of the results would not be possible without a substantial parallel theoretical effort. Such an effort was supported with Rockwell International IR&D funds. The results will be published in more detail in the near future,[A1] with a short version having been submitted recently to Materials Evaluation.[A2]

The nearly periodic roughness of the real slip steps will be represented by a modulation of the oxide-metal interface as shown in Fig. A1; the interface is given by a profile $\eta(x)$,

$$z = \eta(x) = h \cos(2\pi x/d) \ . \qquad (1)$$

It is certainly not essential to the theory given below that the slip steps produce an $\eta(x)$ which is a simple sinusoid (Eq. 1), nor that they be perfectly periodic. For the theory to be a reasonably good representation of the effects of plastic deformation on the surface electromagnetic modes it is necessary merely that the Fourier transform of η be moderately peaked about some wavevector K which can be estimated to be:

$$K \cong 2\pi/\bar{d} \ . \qquad (2)$$

with $\bar{d}$ an average slip step spacing.

There are two families of surface electromagnetic normal modes associated with this oxide layer-metal system; a wholly transverse (light-like) wave which does not exist in the absence of the oxide layer, and

a mode (the surface plasmon) which becomes a longitudinal wave (parallel to the surface) in the absence of the oxide layer. At least in aluminum,[A3] the transverse mode dispersion curve does not permit a significant resonant absorption. This calculation treats only the more important plasmon mode, although it is not difficult to extend the formalism to treat the other mode.

The normal modes of interest are surface transverse magnetic modes propagating in the x direction. Whatever the detailed form of the solution, the periodicity requires that the nonvanishing field components F(E_x, E_z, and H_y) can be chosen in the Bloch form,

$$F(\omega,x,z) = e^{iqx} f(\omega,q,x,z) \ , \tag{2}$$

where f is periodic in x with period d, and

$$-\pi/d \leq 2q \leq \pi/d \ . \tag{3}$$

Thus f can be expanded in a Fourier series in x,

$$f(\omega,q,x,z) = \sum_{n=-\infty}^{\infty} \exp(2in\pi x/d) f_n(\omega,q,z) \ . \tag{4}$$

The periodicity couples the waves with different values of "n", so no one of them is a normal mode. However, since the periodic roughness due to slip bands is slight (typically a few atomic steps in height), the coupling is weak, and the individual terms in the sum (Eq. 4) on n can be almost stable modes.

The mathematical solution of Maxwell's equations utilizes several features of the approach of Kliewer and Fuchs[A4] to the calculation of the anamolous skin effect. Their calculation dealt with a semi-infinite metal with a clean, flat surface and a dielectric response function $\varepsilon_{ij}(\omega,\underset{\sim}{q})$ given by:

$$\varepsilon_{ij}(\omega,\underset{\sim}{q}) = (\delta_{ij} - \frac{q_i q_j}{q^2})\,\varepsilon_t + \frac{q_i q_j}{q^2}\,\varepsilon_\ell \qquad (5)$$

where ε_t and ε_ℓ are, respectively, the transverse and longitudinal dielectric functions. To obtain analytic solutions to the coupled equations introduced by the "slip-steps", and to treat absorption in some detail, the classical limit of this dielectric function was employed in these calculations; that is,

$$\varepsilon_t(\omega,q) \cong \varepsilon_\ell(\omega,q) \cong \varepsilon(\omega)\ , \qquad (6)$$

where $\varepsilon(\omega)$ is complex for both metal and oxide.

The naive expectation is that this approximation is certainly valid because the wavevectors of interest ($\sim \pi/d \sim 50\mu m^{-1}$) are very small compared to the Fermi wavevector ($\sim 1.75 \times 10^4 \mu m^{-1}$). Though this argument has merit, it is not completely convincing, for there is reason[A5] to believe the surface photoeffect is significantly affected by nonlocality (the q dependence of $\varepsilon(\omega,q)$) even at these long wavelengths. However, the purpose of this calculation is to determine the effects of the slip steps in the simplest reasonable model, thereby, it is hoped, helping to establish the mechanism for the observed deformation enhanced photoyield.

The slip steps are most conveniently treated by a prescription introduced by Maradudin and Mills[A6] to study scattering and absorption of electromagnetic radiation by a rough surface. The dielectric function for both metal (ε_M) and oxide (ε_d) can be written in the form:

$$\varepsilon(\omega) = \varepsilon_M(\omega)\ \theta(z-\eta(x)) + \varepsilon_d(\omega)\ \theta(\eta(x)-z)\ , \tag{7}$$

where θ is the Heaviside unit step function. Following Maradudin and Mills, we expand the step functions in power of η,

$$\varepsilon(\omega) = \varepsilon_M(\omega)\theta(z) + \varepsilon_d(\omega)\theta(-z) + (\varepsilon_d(\omega) - \varepsilon_M(\omega))\ \eta(x)\delta(z)\ , \tag{8}$$

where terms of order η^2 have been discarded.

Although in the local approximation (Eq. 6) the electric field is divergence-free except at boundaries, the treatment of the boundaries given here makes it desirable to write Maxwell's equations in the form:

$$(\nabla^2 + \frac{\omega^2}{c^2})\underset{\sim}{E} - \nabla(\nabla\cdot\underset{\sim}{E}) = \frac{-4\pi\omega^2}{c^2}\ \underset{\sim}{P} \tag{9}$$

where the general polarization density $\underset{\sim}{P}$ includes the electric current $\underset{\sim}{J}$. In terms of the decomposition given by Eq. 2 and Eq. 4, Eq. 9 becomes:

$$\frac{d^2E_{n,x}}{dz^2} + \frac{\omega^2}{c^2}\ E_{n,x} - i(q+K_n)\ \frac{dE_{n,z}}{dz} = -\ \frac{4\pi\omega^2 P_{n,x}}{c^2} \tag{10a}$$

and

$$[\frac{\omega^2}{c^2} - (q+K_n)^2]E_{n,z} - i(q+K_n)\ \frac{dE_{n,x}}{dz} = -\ \frac{4\pi\omega^2 P_{n,z}}{c^2}\ , \tag{10b}$$

where the "reciprocal lattice" vector K_n is given by:

$$K_n = 2n\pi/d\ . \tag{11}$$

Let us consider first the metal ($z>0$). This is most easily solved by utilizing the observation of Kliewer and Fuchs[A4] that the infinite half space can be replaced by a corresponding problem in an infinite medium with a spatial symmetry. That symmetry arises from the requirement that

the electrons be reflected at the metal surface and is given by:

$$E_x(-z) = E_x(z) \tag{12a}$$

$$D_x(-z) = D_x(z) \tag{12b}$$

$$E_z(-z) = -E_z(z) \tag{12c}$$

$$D_z(-z) = -D_z(z) . \tag{12d}$$

Although Kliewer and Fuchs obtained this condition from a Boltzmann equation description of specularly reflected electrons, it can also describe this periodic potential reflection which permits the electrons to gain or lose multiples of momentum $\hbar K_n$ parallel to the surface as shown in Fig. A2. Thus we imagine the metal to be the upper part of an infinite metal with a "picket fence" at z = 0, and with no electron transfer across z = 0. With the addition of this fictitious metal in the lower half space, Eq. 10 can be Fourier transformed. Because of the conditions 12, dE_x/dz and E_z have discontinuities at z = 0, so the Fourier transforms are:

$$\int_{-\infty}^{\infty} dz \exp(-iq_3 z) \frac{d^2E_x}{dz^2} = -q_3^2 \hat{E}_{n,x}(q_3) - 2 \frac{dE_{n,x}(0^+)}{dz} \tag{13}$$

and

$$\int_{-\infty}^{\infty} dz \exp(-iq_3 z) \frac{dE_{n,z}}{dz} = iq_3 \hat{E}_n(q_3) - 2E_{n,z}(0^+) . \tag{14}$$

By utilizing $\nabla \times \underset{\sim}{E} = i\omega \underset{\sim}{H}/c$, Eq. 10 becomes:

$$[\frac{\omega^2 \varepsilon}{c^2} - q_3^2]\hat{E}_{n,x} + q_3(q+K_n)\hat{E}_{n,z} = 2i\omega H_{n,y}(0^+)/c - \tfrac{1}{2}\omega^2 h\Delta\varepsilon(E_{n-1,x}(0^+) + E_{n+1,x}(0^+)/c^2 \tag{15a}$$

and

$$[\frac{\omega^2}{c^2} - (q+K_n)^2]\hat{E}_{n,z} + q_3(q+K_n)\hat{E}_{n,x} = 0 . \tag{15b}$$

The absence of a contribution to the right side of Eq. 15b from the delta function perturbation is a consequence of the antisymmetry of E_z about z = 0. These two equations are easily solved to give:

$$\hat{E}_{n,x}(q_3) = \frac{+2ic}{\omega\varepsilon} \frac{\alpha_n^2}{q_3^2+\alpha_n^2} \{H_{n,y}(0^+) + \frac{i\omega}{4c} h\Delta\varepsilon(E_{n-1,x}(0^+) + E_{n+1,x}(0^+)\} , \quad (16)$$

where α_n is given by

$$\alpha_n^2 = (q+K_n)^2 - \omega^2\varepsilon/c^2 . \quad (17)$$

The inverse Fourier transform is elementary, and is conveniently written in the form:

$$E_{n,x}(z) = \frac{ic\alpha_n}{\omega\varepsilon} e^{-\alpha_n z}\{H_{n,y}(0^+) + B_{nm} E_m(0^+)\} \quad (18)$$

where the matrix $\underset{\sim}{B}$ is used with the summation convention and is defined by

$$B_{nm} = \frac{i\omega h\Delta\varepsilon}{4c} (\delta_{n,m+1} + \delta_{n,m-1}) . \quad (19)$$

The quantity Z_p defined by

$$Z_p = \frac{ic\alpha_n}{\omega\varepsilon} \quad (20)$$

is the classical surface impedance (p - polarized light) of a metal. Equation 18 is formally solved by

$$E_{n,x}(0) = (Z_p^{-1}-\underset{\sim}{B})^{-1}_{nm} H_{m,y}(0^+) = Z^M_{nm}H_{m,y}(0^+) \quad (21)$$

which defines a matrix surface impedance $\underset{\sim}{Z}^M$ in the presence of the periodic coupling represented in $\underset{\sim}{B}$. This completes the description of the metal.

The description of the oxide is considerably more complicated because of the presence of two boundaries, a difficulty only partially alleviated by treating (unrealistically) the oxide-vacuum interface as a plane normal

to the z axis. It has been shown[A7] that even for normally incident light there are significant modifications when both interfaces are rough. They are unlikely, however, to alter the qualitative conclusions obtained from this idealized geometry.

It is again very useful to imagine that the medium is in contact with a symmetric counterpart, in this case extending over the region $0 \leq z \leq a$, and satisfying the reflection conditions of Eq. 12. The solution to Eq. 10 is similar, but now requires a Fourier series in z, i.e.,

$$\hat{\underset{\sim}{E}}_n(\omega,q,\tfrac{\ell\pi}{a}) = \int_{-a}^{a} dz\, \exp(-i\ell\pi z/a)\, \underset{\sim}{E}_n(\omega,q,z) \ . \tag{22}$$

Maxwell's equations have the slightly different form:

$$[\frac{\omega^2\varepsilon_d}{c^2} - (\tfrac{\ell\pi}{a})^2]\, \hat{E}_{n,x}(\tfrac{\ell\pi}{a}) + \tfrac{\ell\pi}{a}\,(q+K_n)\, \hat{E}_{n,z}(\tfrac{\ell\pi}{a})$$

$$= \frac{-2i\omega}{c}\,\{H_{n,y}(0^-) - e^{-i\ell\pi}H_{n,y}(-a) + B_{nm}E_m(0)\} \tag{23a}$$

and

$$[\frac{\omega^2\varepsilon_d}{c^2} - (q+K_n)^2]\, \hat{E}_{n,z}(\tfrac{\ell\pi}{a}) + \tfrac{\ell\pi}{a}\,(q+K_n)\, \hat{E}_{n,x}(\tfrac{\ell\pi}{a}) = 0 \ . \tag{23b}$$

The choice of $e^{-i\ell\pi}$ (rather than, e.g., $e^{+i\ell\pi}$ or $e^{-5i\ell\pi}$) simplifies certain formulas in the inversion of the Fourier series. Proceeding as before, one obtains:

$$E_{n,x}(z) = \frac{-ic\beta_n}{\omega\varepsilon_d}\,\{[H_{n,y}(0^-) - B_{nm}E_{m,x}(0)]\, S_1(z) - H_{n,y}(-a)\, S_2(z)\} \tag{24}$$

where

$$\beta_n^{\,2} = (q+K_n)^2 - \omega^2\varepsilon_d/c^2 \tag{25}$$

and the Fourier sums S_1 and S_2 are defined by

$$S_1(z) = \frac{\beta_n a}{\pi^2} \sum_{\ell=-\infty}^{\infty} \frac{\exp(i\ell\pi z/a)}{\ell^2 + (\beta_n a/\pi)^2} \tag{26}$$

and

$$S_2(z) = S_1(z-a) \ . \tag{27}$$

To evaluate these sums we introduce a contour integral in the complex "ℓ" plane. The sums are to be the residues of an analytic function of a complex variable "s" with simple poles at each integer "ℓ". A suitable function (for S_1) is:

$$f(s) = \exp(is\pi z/a)/[(\exp(-2\pi is)-1)(s^2 + (\beta_n a/\pi)^2)] \ . \tag{28}$$

The choice $\exp(-2\pi is)$ enables us to add to the integral the integrals over the dashed semicircles at ∞ shown in Fig. A3 (remember that $z<0$). The function $f(s)$ is ambiguous by multiples of $\exp(2n\pi is)$ where "n" is any integer. This ambiguity is eliminated by the two physical requirements that as the oxide becomes infinitely thick the coefficient S_2 of $H_{n,y}(-a)$ must vanish, and the coefficient S_1 of $H_{n,y}(0^-)$ must include only exponentially decreasing terms in $z(\sim\exp(+\beta_n z))$. The unique value of "n" which satisfies these conditions is $n = 0$. (This particularly simple choice is a consequence of our choice of $\exp(-i\ell\pi)$ in Eq. 23a.)

The sum S_1 can easily be obtained now by deforming the contours to enclose the simple poles at $s = \pm i\beta_n a/\pi$, and the result is:

$$S_1(z) = \oint ds\ f(s) = \cosh\ \beta_n(a+z)\ \operatorname{csch}\ \beta_n a \ . \tag{29}$$

Thus Eq. 24 becomes

$$E_{n,x}(z) = \frac{-ic\beta_n}{\omega\varepsilon_d} \operatorname{csch}\ \beta_n a\{[H_{n,y}(0^-) - B_{nm}E_{m,x}(0)] \cosh\ \beta_n(a+z) - H_{n,y}(-a) \cosh\ \beta_n \} \ .$$

$E_{m,x}(0)$ can be eliminated by evaluating Eq. 30 at z = 0 and defining a matrix $\underset{\sim}{A}$ by

$$A^{-1}_{nm} = \delta_{nm} - ic\beta_n B_{nm}/(\omega\varepsilon_d \tanh \beta_n a) . \tag{31}$$

The electric field is then given in terms of the boundary values of the magnetic field by:

$$E_{n,x}(z) = M_{nm}(z)H_{m,y}(0^-) - V_{nm}(z)H_{m,y}(-a) , \tag{32}$$

where the matrices M and V are defined by

$$M_{nm}(z) = \frac{-ic\beta_n \cosh \beta_n(a+z)}{\omega\varepsilon_d \sinh \beta_n a} [\delta_{nm} + \frac{ic}{\omega\varepsilon_d} (\underset{\sim}{BA})_{nm} \beta_m \operatorname{ctnh} \beta_m a] \tag{33}$$

and

$$V_{nm}(z) = \frac{-ic\beta_n \cosh \beta_n z}{\omega\varepsilon_d \sinh \beta_n a} [\delta_{nm} + \frac{ic}{\omega\varepsilon_d} \frac{\cosh \beta_n(a+z)}{\cosh \beta_n z} \frac{(\underset{\sim}{BA})_{nm} \beta_m}{\sinh \beta_m a}] . \tag{34}$$

In the vacuum below the oxide the ratio of transverse electric to magnetic fields is simply the diagonal matrix $Z_v(n)$,

$$E_{n,x}/H_{n,y} = \frac{-ic}{\omega} ((K_n+q)^2 - \omega^2/c^2)^{\frac{1}{2}} \equiv Z_v(n) . \tag{35}$$

The transverse (x and y) electric and magnetic field components are, of course, continuous across the boundaries, so by evaluating Eq. 32 at z=0 and z=-a, one can use Eq. 35 and Eq. 21 to eliminate the electric fields, thereby obtaining two matrix equations relating the vectors $H_{n,y}(0)$ and $H_{n,y}(-a)$. From these relations one can eliminate $H_{n,y}(-a)$ to obtain:

$$(R_{nm} - \delta_{nm})H_{m,y}(0) = 0 \tag{36}$$

where

$$\underset{\sim}{R} = (\underset{\sim}{M}(0) - \underset{\sim}{Z_M})^{-1}\underset{\sim}{V}(0)(\underset{\sim}{V}(-a) + Z_v)^{-1}\underset{\sim}{M}(-a) . \tag{37}$$

This leads to a very simple prescription for calculation of the dispersion curves $\omega_j(q)$ of the surface plasmons in the presence of this periodic perturbation. The criterion is that $\omega_j(q)$ be a root of the transcendental equation:

$$\lambda_j(\omega_j(q),q) - 1 = 0 \tag{38}$$

where $\lambda_j(\omega,q)$ is the $j^{\underline{th}}$ eigenvalue of R.

The roots were found numerically for aluminum to zeroth order in the perturbation. The effect of the perturbation on the dispersion curve can be neglected except where two roots are nearly degenerate. At such a symmetry point the secular equation is of the form:

$$(\omega-\omega^o(q))^2 - (ah\Delta\varepsilon)^2 = 0 \tag{39}$$

where "a" is a real constant and h is the amplitude of the surface modulation. The roots are thus

$$\omega = \omega^o(q) \pm ah\Delta\varepsilon \ . \tag{40}$$

The results were calculated using parameterizations of the empirical complex dielectric functions of Al[A8] and Al_2O_3.[A9] The lifetimes were also obtained, producing a width to the dispersion curves of about ½eV which was not very sensitive to q in the region of interest. The results are shown in Fig. A4.

The physical consequences of these dispersion curves are apparent from comparison to the dispersion curve for light, shown also in Fig. A4. The light is incident from below in the xz plane, and satisfies $\omega = cq \csc\theta$ (remember that q is the x component of the wave vector). If the light is p-polarized (electric vector in the xz plane), it can couple resonantly

through the periodic susceptibility (the third term in Eq. 8) to the plasmon modes whenever their dispersion curves cross. These resonant absorption peaks should produce corresponding increases in the photoyield. The effect of increased deformation is to increase the area of slip step creation, but not their separation, as was discussed in the present report (Discussion of Experimental Results, Section 4.0). Thus the photoyield should increase with increasing deformation, but the photon energy for maximum effect should change little.

The lowest lying branch ($n = 0$) in Fig. A4 corresponds to fields with x dependence given by $\exp(iqx)$, the next band $\exp(i(q-2\pi/d)x)$, and the highest band $\exp(i(q+2\pi/d)x)$. As mentioned earlier, the quantitative shift due to the oxide layer is large, with the highest band shifted down by a factor of about $(2/(1+\varepsilon(\omega)))^{\frac{1}{2}} \simeq 0.6$ from the corresponding band on an oxide-free surface. This result is almost independent of oxide thickness provided that thickness is greater than 50Å. The results are somewhat sensitive to the actual optical properties of the oxide layer, which may differ somewhat from crystalline Al_2O_3.[A9] The qualitative effect of polycrystalline rather than crystalline aluminum oxide is to reduce the dielectric function, shifting the upper curve up slightly.

If the surface plasmon coupling is indeed the mechanism for the fatigue enhancement, the increase in photoyield should occur as a rather broad peak around the resonance energy. The photoyield, however, is rapidly varying in that energy region due to two other effects, the proximity to the work function, and a classical interference effect[A3] in the absorption due to the oxide layer. To reduce the bias in the energy dependence due to these two effects, the data was divided by the photoyield

in the metal calculated without roughness and averaged over the two polarizations. This calculation was carried out by calculating the energy absorbed at depth z, multiplying by a probability ½ exp(-z/L) of reaching the surface, and a factor exp(-a/L') for transmission through the oxide, then integrating over depth. Approximate empirical values were used for the attenuation lengths L, L'. This is a fairly crude approach, but the predicted flat surface values were within a factor of 2-3 of the experiment, and should reasonably account for the purely classical wavelength dependence. The change with number of fatigue cycles N is shown in Fig. A5, exhibiting two rather broad peaks which increase in height but do not change in energy as deformation progresses. The smooth curve is a spline fit. This normalized data does exhibit two peaks, as expected from Fig. A4. The higher energy peak is about 1 eV higher than expected, but this may be due to the uncertainty about the optical properties of the actual oxide. Quantitative inclusion of the small shift due to the slip steps would also shift the theoretical prediction upward. In contrast to the results of Endriz and Spicer,[A3] the locations of the peaks appear not to shift with increasing roughness. This is expected from the model, since fatigue increases the area covered by slip steps, but does not appreciably change their spacing.

To demonstrate this effect in detail, the above work was extended to calculate the absorption by the aluminum in the presence of this periodic roughness. To simplify the numerical calculation, only the first two terms (n = 0, -1) were retained. The resulting absorption is shown in Fig. A6 for assumed roughness amplitudes of 1 and 15A. There is no effect for 1A, and a maximum enhancement of a factor of about 3 for 15A. Moreover,

this occurs at about the right energy for the lowest peak observed in the experimental data (Fig. A5). The calculation will be extended in the near future to include the higher bands. It is clear from these results and the dispersion curve, Fig. A4, that this will produce a second peak about 1 eV higher, in agreement with the experiment. Although the precise height of the slip steps is unkonwn, a value of 3-5 lattice constants (12-20A) is reasonable. The theoretical calculation demonstrates that a reasonable assumption about the amplitude of the slip steps, the observed spacing of the slip steps, and the measured oxide layer thickness, lead to a predicted enhancement of the absorption of about the right magnitude at the right energies. Since the theory is rather sensitive to slip step height and spacing (1000A spacing shifts the peak to 5.3 eV), this agreement seems to be convincing evidence for the plasmon mechanism.

REFERENCES - APPENDIX

A1. W. J. Pardee and O. Buck, to be submitted to Appl. Phys.

A2. W. J. Pardee and O. Buck, Materials Evaluation - Research Supplement (accepted for publication).

A3. W. J. Pardee, in preparation.

A4. K. L. Kliewer and R. Fuchs, Phys. Rev., 172, 607 (1968).

A5. K. L. Kliewer, Phys. Rev., B14, 1412 (1976).

A6. A. A. Maradudin and D. L. Mills, Phys. Rev., B11, 1392 (1975).

A7. D. L. Mills and A. A. Maradudin, Phys. Rev., B12, 2943 (1975).

A8. H. Ehrenreich, H. R. Phillip, and B. Segall, Phys. Rev., 132, 1918 (1963).

A9. E. T. Arakawa and M. W. Williams, J. Phys. Chem. Solids, 29, 735 (1968).

A10. G. J. Endriz and W. E. Spicer, Phys. Rev., B4, 4159 (1971).

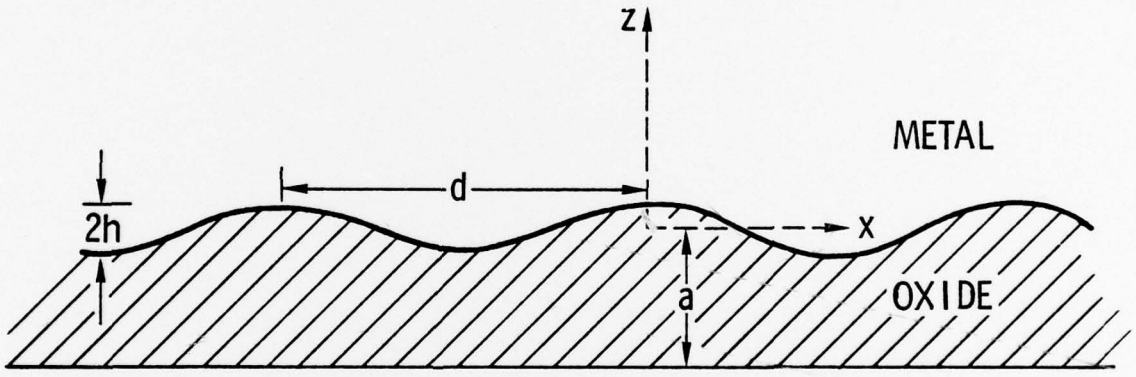


Fig. A1 Diagram of the coordinate system illustrating the sinusoidal roughness at the metal-oxide interface.

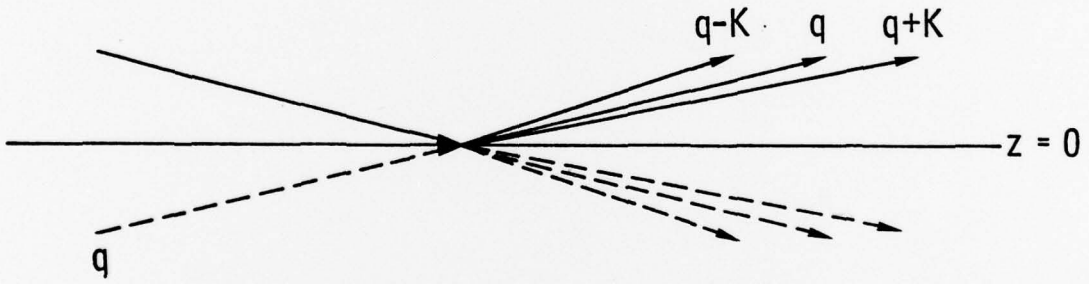


Fig. A2 Illustration of the symmetry condition on the electron current diffracted by the picket fence in the equivalent infinite medium, $J_x(z) = J_x(-z)$, $J_z(-z) = -J_z(z)$.

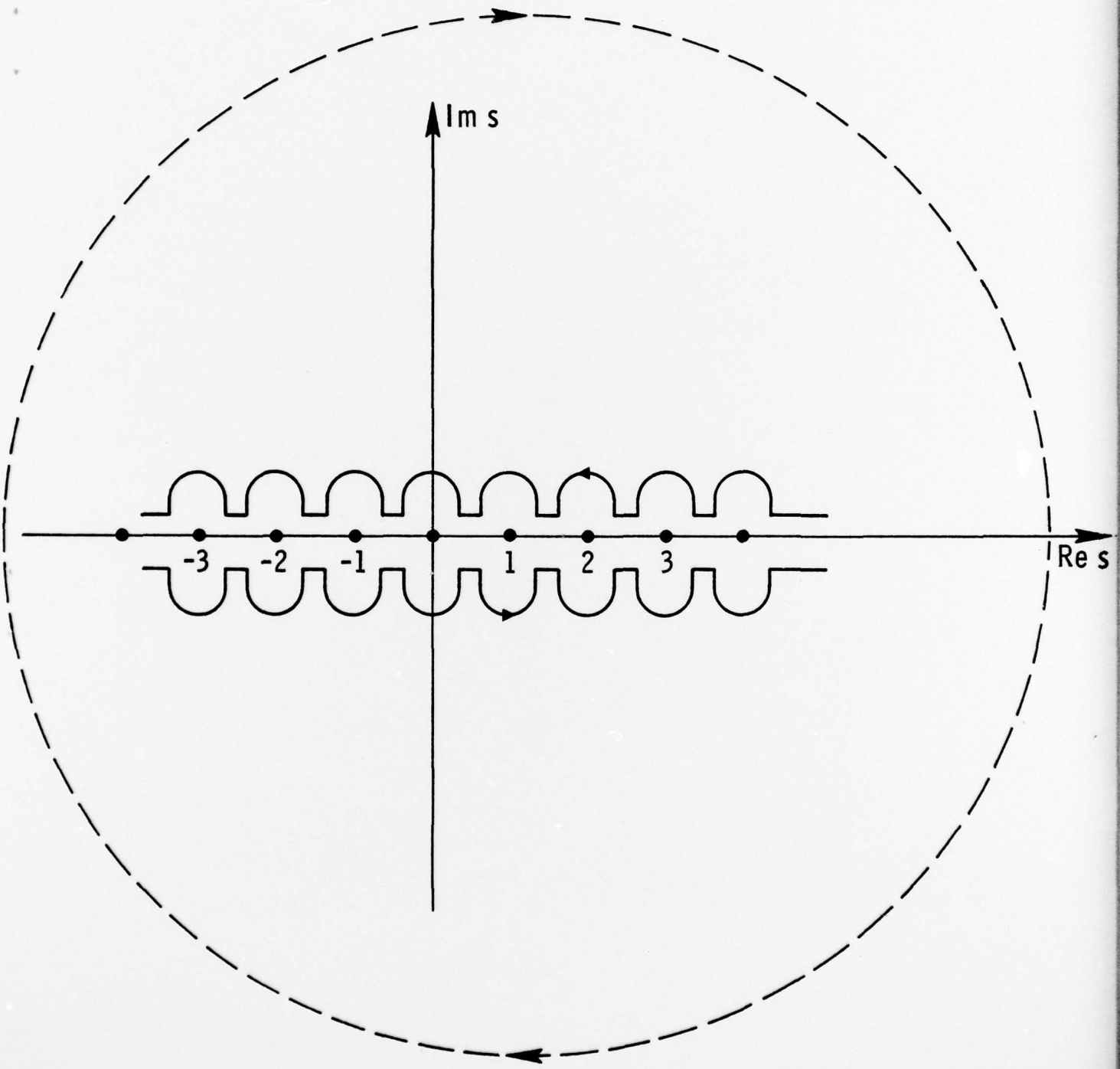


Fig. A3 Integration contour used to invert the Fourier sums in the variable conjugate to z.

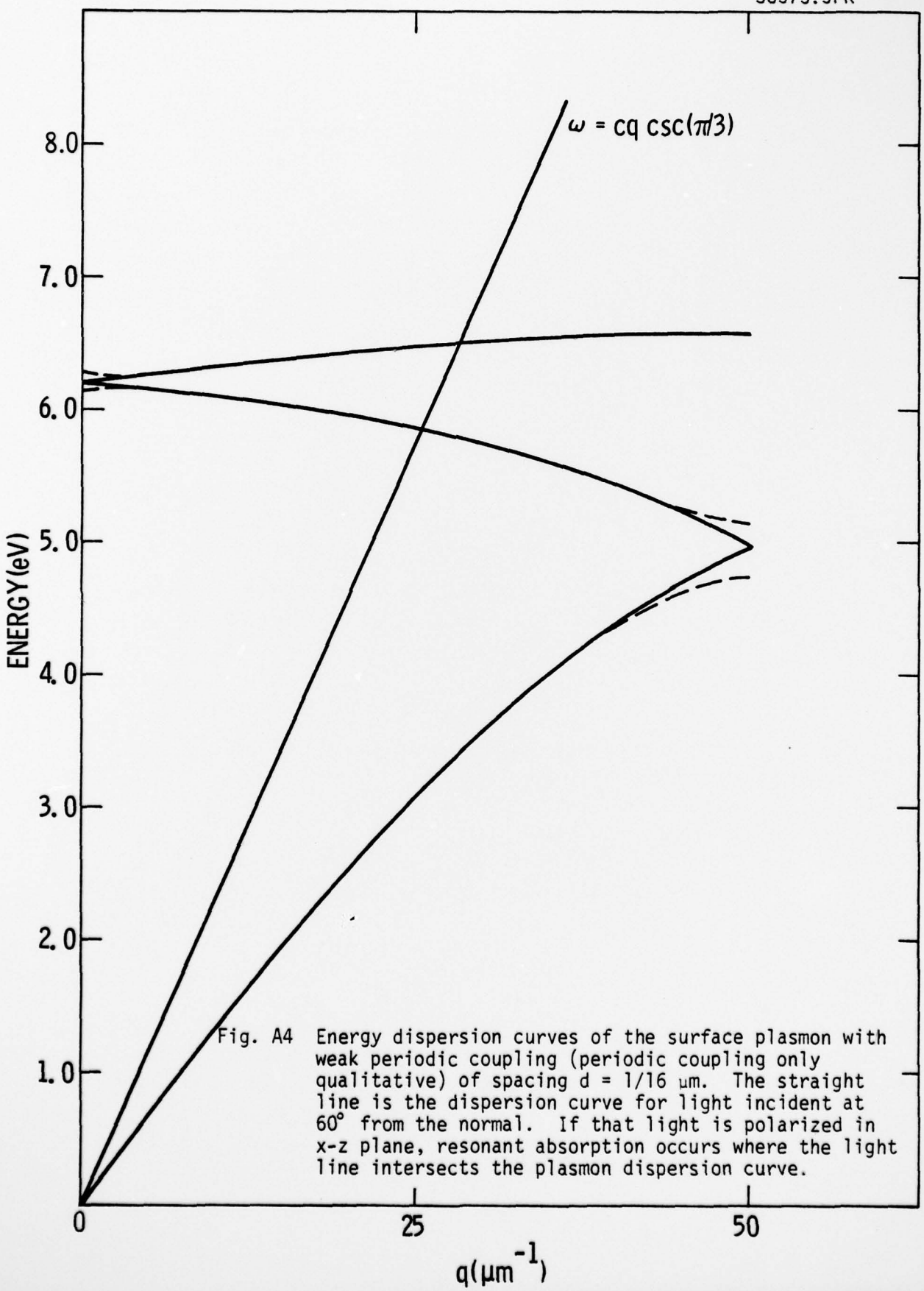


Fig. A4 Energy dispersion curves of the surface plasmon with weak periodic coupling (periodic coupling only qualitative) of spacing d = 1/16 μm. The straight line is the dispersion curve for light incident at 60° from the normal. If that light is polarized in x-z plane, resonant absorption occurs where the light line intersects the plasmon dispersion curve.

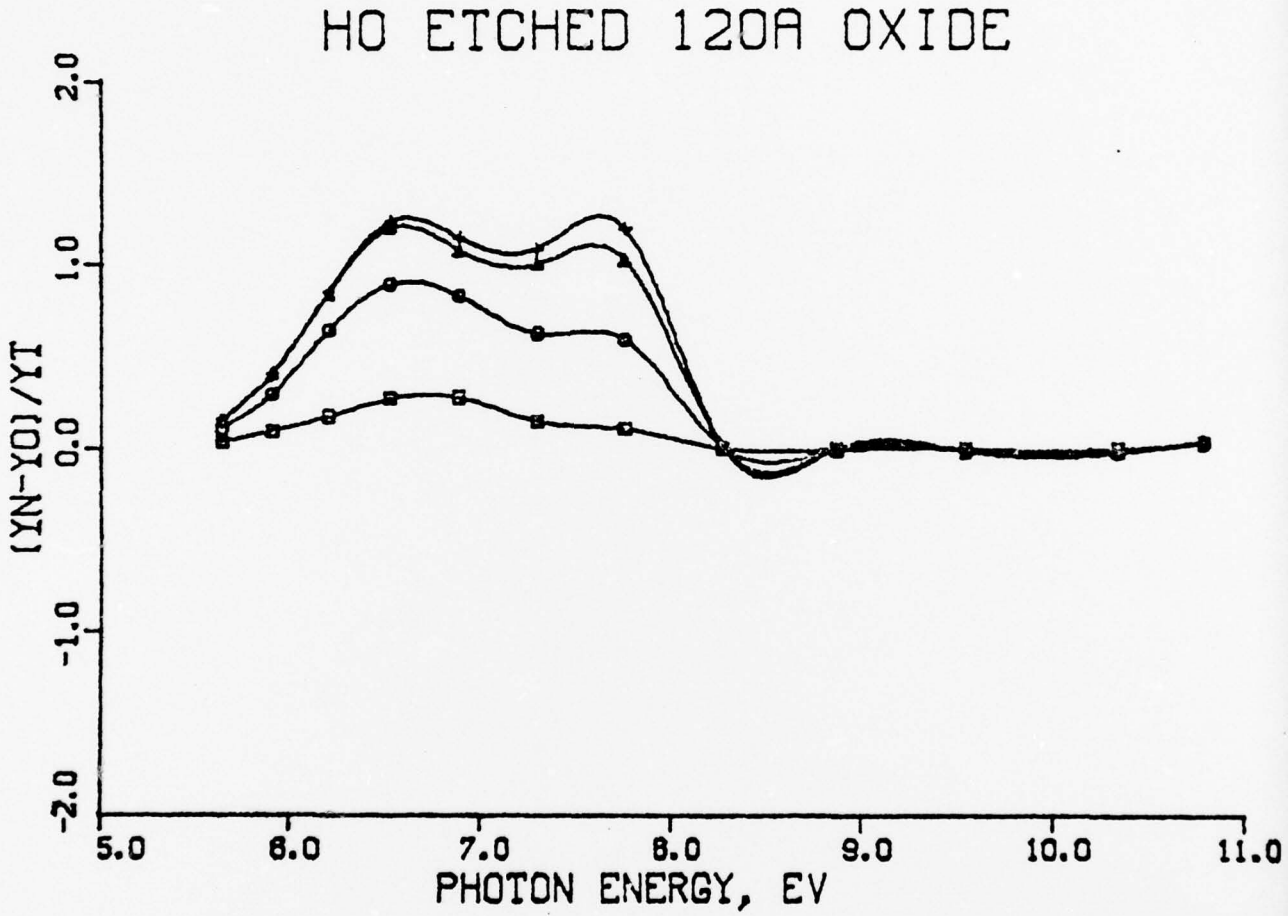


Fig. A5 The change in photoyield of Al 1100 HO, normalized by the calculated photoyield in metal (oxide layer 120Å thick). Data calculated using raw data shown in Fig. 7 of the report.

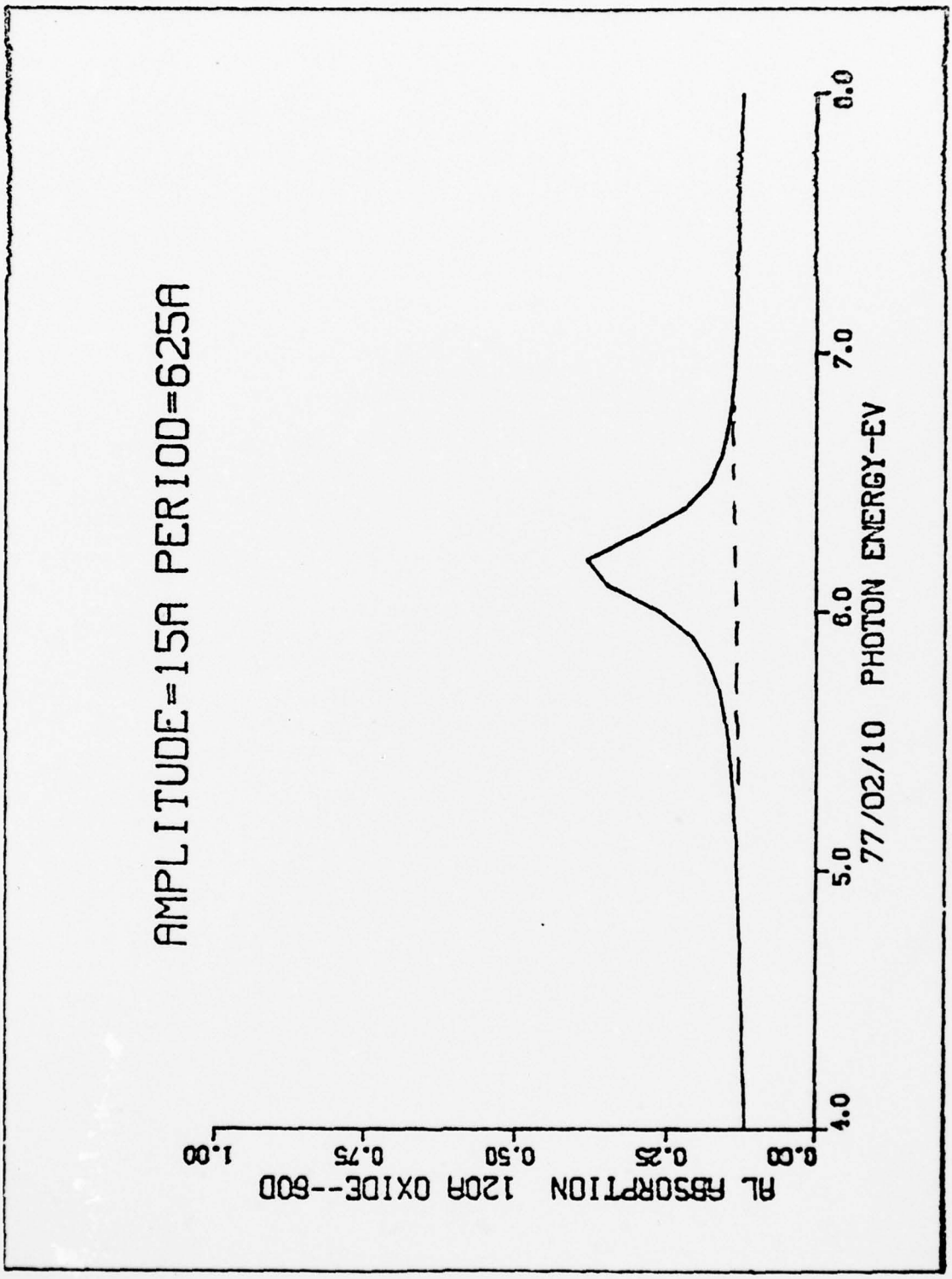


Fig. A6 Theoretical prediction of absorption of aluminum with periodically oscillating surface of amplitude 15A and period 625A and with an oxide layer 120Å thick for P polarized light incident at 60° from the normal. The dashed curve is the absorption with the surface oscillation assumed to be only 1A, and is indistinguishable from that of a flat surface. This calculation retained only the first resonance; retention of additional terms would produce a second peak about 1 eV higher in photon energy.